

SPECTRAL CHARACTERISTICS AND CORRECTION OF LONG-TERM EDDY-COVARIANCE MEASUREMENTS OVER TWO MIXED HARDWOOD FORESTS IN NON-FLAT TERRAIN

HONG-BING SU^{1,*}, HANS PETER SCHMID¹, C. S. B. GRIMMOND¹, CHRISTOPH
S. VOGEL² and ANDREW J. OLIPHANT^{1,3}

¹Indiana University, Bloomington, IN, U.S.A.; ²University of Michigan Biological Station, Pellston,
MI, U.S.A.; ³San Francisco State University, San Francisco, CA, U.S.A.

(Received in final form 17 March 2003)

Abstract. We present turbulence spectra and cospectra derived from long-term eddy-covariance measurements (nearly 40,000 hourly data over three to four years) and the transfer functions of closed-path infrared gas analyzers over two mixed hardwood forests in the mid-western U.S.A. The measurement heights ranged from 1.3 to 2.1 times the mean tree height, and peak vegetation area index (VAI) was 3.5 to 4.7; the topography at both sites deviates from ideal flat terrain. The analysis follows the approach of Kaimal et al. (*Quart. J. Roy. Meteorol. Soc.* **98**, 563–589, 1972) whose results were based upon 15 hours of measurements at three heights in the Kansas experiment over flatter and smoother terrain. Both the spectral and cospectral constants and stability functions for normalizing and collapsing spectra and cospectra in the inertial subrange were found to be different from those of Kaimal et al. In unstable conditions, we found that an appropriate stability function for the non-dimensional dissipation of turbulent kinetic energy is of the form $\phi_\epsilon(\zeta) = (1 - b^{-\zeta})^{-1/4} - c^{-\zeta}$, where ζ represents the non-dimensional stability parameter. In stable conditions, a non-linear function $G_{xy}(\zeta) = 1 + b_{xy}\zeta^{c_{xy}}$ ($c_{xy} < 1$) was found to be necessary to collapse cospectra in the inertial subrange. The empirical cospectral models of Kaimal et al. were modified to fit the somewhat more (neutral and unstable) or less (stable) sharply peaked scalar cospectra observed over forests using the appropriate cospectral constants and non-linear stability functions. The empirical coefficients in the stability functions and in the cospectral models vary with measurement height and seasonal changes in VAI. The seasonal differences are generally larger at the Morgan Monroe State Forest site (greater peak VAI) and closer to the canopy.

The characteristics of transfer functions of the closed-path infrared gas analysers through long-tubes for CO₂ and water vapour fluxes were studied empirically. This was done by fitting the ratio between normalized cospectra of CO₂ or water vapour fluxes and those of sensible heat to the transfer function of a first-order sensor. The characteristic time constant for CO₂ is much smaller than that for water vapour. The time constant for water vapour increases greatly with aging tubes. Three methods were used to estimate the flux attenuations and corrections; from June through August, the attenuations of CO₂ fluxes are about 3–4% during the daytime and 6–10% at night on average. For the daytime latent heat flux (Q_E), the attenuations are found to vary from less than 10% for newer tubes to over 20% for aged tubes. Corrections to Q_E led to increases in the ratio $(Q_H + Q_E)/(Q^* - Q_G)$ by about 0.05 to 0.19 (Q_H is sensible heat flux, Q^* is net radiation and Q_G is soil heat flux), and thus are expected to have an important impact on the assessment of energy balance closure.

Keywords: Cospectral correction, Cospectral model, Energy balance, Forest, Spectral characteristics, Transfer function.

* Corresponding author address: Department of Geography, East Carolina University, Greenville, NC 27858-4353, U.S.A. E-mail: suh@mail.ecu.edu



Boundary-Layer Meteorology **110**: 213–253, 2004.
© 2003 Kluwer Academic Publishers. Printed in the Netherlands.

1. Introduction

High frequency loss in measured eddy-covariance fluxes can be caused by path/line averaging, sensor separation, inadequate sensor frequency response, damping through tubes in closed-path gas analyzers, and filtering in data processing (Moore, 1986). Previous studies using spectral methods have shown that corrections to measured fluxes range from a few to over 30% (Eugster and Senn, 1995; Leuning and Judd, 1996; Horst, 1997; Massman, 2000). The magnitudes of such flux losses in the higher frequency range can be of the same order as unaccounted for lower frequency flux contributions due to inadequate averaging time (Rimann and Tetzlaff, 1994; Sakai et al., 2001; Finnigan et al., 2003).

Spectral methods to correct flux losses often require knowledge of the true cospectra, as well as the transfer functions (Moore, 1986; Massman, 2000). The most commonly used cospectral models in the atmospheric surface layer are those of Kaimal et al. (1972) and Wyngaard and Coté (1972), derived from the Kansas experiment over a relatively smooth surface and flat terrain. However, the heights of eddy-covariance systems at most long-term AmeriFlux forest sites are about twice the canopy height or less. Thus, they are in the so-called roughness sublayer where tree elements impose strong influences on the flow characteristics, and the validity of surface-layer Monin–Obukhov similarity becomes questionable (Kaimal and Finnigan, 1994). Moreover, the topography at most flux sites is not flat. Therefore, there is a need to evaluate the characteristics of turbulence spectra and cospectra over forest canopies, and to compare them with the standard Kansas experiment results.

Some previous studies presented spectra and cospectra in and above plant canopies (Shaw et al., 1974; Anderson et al., 1986; Baldocchi and Meyers, 1988; Amiro, 1990). However, their emphases were on spectra inside canopies in comparison with those above, and the above canopy spectra or cospectra were not analyzed in the same way as Kaimal et al. (1972) for comparison. These short-term campaign studies were based on relatively limited data compared to nearly 40,000 hr of measurements from the two long-term AmeriFlux sites used in this study. As noted in Wyngaard and Coté (1972), the results of Kaimal et al. (1972) were also based upon very sparse data (15 1-hr runs, 10 unstable, 5 stable, at three heights). However, the Kansas experiment provided a more complete measurement set, including the vertical profiles of mean wind speed and temperature, and the dissipation of turbulent kinetic energy (TKE) (among other variables) that was used in the analyses of Kaimal et al. (1972). These complementary measurements are not available for the present study. Sakai et al. (2001) analyzed cospectra using the long-term AmeriFlux measurements over Harvard Forest but focused only on convective conditions. They reported that the normalized cospectra of momentum and of a scalar in the roughness sublayer over forest canopies are more sharply peaked than those observed in the Kansas experiment (Kaimal et al., 1972) and may be described by a single form in convective conditions.

This study analyses data from long-term measurements over two mixed hardwood forests, one at the University of Michigan Biological Station (UMBS) in northern lower Michigan, U.S.A. ($45^{\circ}36'$ N, $84^{\circ}43'$ W), and the other at the Morgan Monroe State Forest (MMSF) in south-central Indiana, U.S.A. ($39^{\circ}19'$ N, $86^{\circ}25'$ W). The two main objectives of this study are to compare spectral and cospectral characteristics over forests with the more 'universally' accepted functions from Kaimal et al. (1972), and to evaluate tube attenuations of eddy-covariance fluxes of CO_2 and water vapour.

In the following, a brief description of the two sites, instruments, measurements, data analyses is given in Section 2; characteristics of spectra and cospectra are discussed in Section 3. Transfer functions and estimates of frequency loss in CO_2 and water vapour fluxes (or Q_E) due to tube damping, and implications of cospectral correction in Q_E on the energy balance closure, are presented in Section 4. The main findings and conclusions are summarized in Section 5.

2. Sites, Data and Processing

A detailed description of the MMSF site, its topography, composition of tree species, soil type, mean canopy height, vegetation area index (VAI), flux tower structure, instrumentation, can be found in Schmid et al. (2000). A similar description of the UMBS site is given in Schmid et al. (2003). Neither site is flat. The MMSF site has a ridge/ravine topography with a relative relief of less than 60 m and an overall fall of 90 m in 4 km. At the UMBS site, the most significant topographic feature is the crest of an interlobate moraine approximately 1 km to the south-west of the flux tower with a relative elevation of about 30 m. Peak VAI was 3.5 at the UMBS site and 4.7 at the MMSF site. For the leafless periods, VAI was about 1 at UMBS and about 1.5 at MMSF, representing stem and branch area, and (in the case of UMBS) some evergreens in the understory. The mean tree height (h_C) was 22 m at UMBS and 26 m at MMSF. The structures of the main flux towers at both sites are identical and approximately 46 m tall.

At each site, eddy-covariance systems, each consisting of a Campbell Scientific, Inc. CSAT3 three-dimensional (3-D) sonic anemometer-thermometer and a closed-path Licor-6262 infrared $\text{CO}_2/\text{H}_2\text{O}$ gas analyzer (IRGA), are installed at two heights, 34 m and 46 m. Thus, the two measurement heights are $1.5h_C$ and $2.1h_C$ at UMBS, $1.3h_C$ and $1.8h_C$ at MMSF. The IRGAs are maintained in climate-controlled laboratories at the base of the towers and sample air is drawn from inlets close to the transducer array of each CSAT3 through long Teflon tubes (4.8×10^{-3} m inner diameter) with lengths of 52 m and 40 m for the 46-m and 34-m systems respectively at the UMBS site, and similarly 56 m and 46 m at the MMSF site. The flow rate at both heights is about 6 l min^{-1} at the UMBS site, and about 8 l min^{-1} at the MMSF site. In this study, time lags determined from maximum lagged correlations were used (Schmid et al., 2000, 2003). All eddy-

covariance measurements are sampled at 10 Hz and saved continuously, except for periods of instrument maintenance. Data analysed in this study include the periods starting March, 1999 at UMBS and March, 1998 at MMSF, to the end of 2001 at both sites.

Quality analyses of the hourly raw 10-Hz data include the detection of 'hard' and 'soft' flags (Vickers and Mahrt, 1997; Schmid et al., 2000, 2003); in this study, hourly data with continuous flags greater than 10 (1 sec in time) and total flags more than 1.7% (1 min) are excluded. This is a more conservative criterion than that used for direct eddy-covariance calculations, as commonly applied for spectral analysis.

Since the topography at both sites is complex, the ensemble averaged streamline coordinate is chosen. A moving bin-average ($\pm 7^\circ$) is performed for vertical rotation angles in each wind direction and it is assumed that the long-term average mean velocity perpendicular to the mean streamline is zero in each wind direction (Lee, 1998; Baldocchi et al., 2000; Finnigan et al., 2003). We also used a modified planar fit method (Paw et al., 2000; Wilczak et al., 2001) to determine the sonic anemometers' tilt angles as functions of azimuth, and found that it yielded negligible differences in eddy-covariance fluxes and cospectra presented here. Upwind directions that likely suffer from flow distortions by the tower and instruments are also excluded. As in Kaimal et al. (1972), hourly records (10 Hz) were used to calculate spectra and cospectra but without using their two-band (higher and lower frequency ranges) approach.

For the results presented here, a simple block-average was used (i.e., no filtering such as linear-detrending or moving-average) in order to keep spectral and cospectral integration over frequencies equal to directly calculated variances and covariances. Some of these covariances are then corrected for tube attenuation of CO₂ and water vapour fluxes as discussed later in Section 4. As noted by Stull (1988) and, more recently Sakai et al. (2001), non-detrended spectra can potentially exhibit red noise effects on the lower frequency end in certain situations (e.g., in convective conditions) or due to an inadequate sampling period. However, the spectral consequences of detrending and filtering of data are always somewhat subjective, and dependent on the procedure. Moreover, it is important to bear in mind that the low frequency end of any given spectrum is subject to great uncertainty (Stull, 1988). We found that linear-detrending yielded negligible effects on directly calculated variances and covariances as well as spectra and cospectra in near-neutral and stable conditions. As the low frequency end of spectra under convective conditions is not the focus of this work, we do not pursue this topic further. However, our preliminary results using longer sampling or averaging periods showed that there are some contributions from periods longer than 1 hr to the covariances in convective conditions, similar to those reported in Sakai et al. (2001) and Finnigan et al. (2003).

In general, spectral and cospectral densities are small in the highest frequency range. Occasional 'spikes' in the 10-Hz data were replaced with the corresponding

hourly mean (zero fluctuation). Hourly spectra and cospectra were smoothed using the procedure described in Kaimal and Finnigan (1994) except for those at the lowest ten frequencies (periods longer than 6 min). Thus, greater scatter is expected in the lowest decade of frequencies. For a given length of sampling or averaging period, spectral and cospectral estimates in the lowest few frequencies are often considered unreliable due to inadequate sampling in general (Kaimal and Finnigan, 1994) and possibly unresolved lower frequencies and red noise in particular, and therefore are often not used in the interpretation (Stull, 1988).

Unlike Kaimal et al. (1972), where measurements at three heights were combined as an ensemble in their analyses, we analyzed our data separately for each of the four measurement heights in the foliated and leafless season. This allows an examination of the effects of height variations in the roughness layer over forest canopies and of seasonal changes and site specific differences in VAI. This approach was possible because of the large amount of data available from long-term measurements at the two sites that include a similar range of stability as in the Kansas experiment. We used data collected in June through August to represent the foliated season at both sites (Table I). November to April at the UMBS site, and November to March at the MMSF site, represent the leafless season. Bud-break is usually earlier at the MMSF site than at the more northern location of the UMBS site (Schmid et al., 2000, 2003).

A frequently used parameter is $\zeta = (z - d)/L$, the non-dimensional buoyancy term in the TKE budget equation, which is also used as a stability parameter in the surface layer (Stull, 1988). Here d is the zero-plane displacement height, and L is the Obukhov length. We used $d = 0.75h_C$ and $d = 0.6h_C$ for the foliated and the leafless seasons, respectively. These values were estimated using the logarithmic wind profile and the CSAT3 sonic anemometer data at both 46 m and 34 m in near-neutral conditions. Sakai et al. (2001) reported similar values of d/h_C for the Harvard Forest. Sensitivity tests, for example, using $d = 0.5h_C$ for the leafless season, yielded negligible changes in the results presented below. At both the UMBS and MMSF sites, the probability distribution density function of ζ is more sharply peaked in the leafless season (Figure 1), indicating relatively more near-neutral cases as expected. Peak densities are at near-neutral conditions in both seasons, but on the stable ($\zeta > 0$) side in the leafless season and on the unstable side ($\zeta < 0$) in the foliated season.

3. Spectral and Cospectral Characteristics

In this section, we follow the approach of Kaimal et al. (1972) in the analysis of spectral and cospectral characteristics so that similarities and differences between the Kansas experiment and our observations over forests may be examined.

TABLE I
 Number of hourly spectra and cospectra for a specific height, season and stability at the UMBS and MMSF sites (total number = 39, 622).

Year	1998		1999		2000		2001							
	$\zeta > 0$	$\zeta < 0$	$\zeta > 0$	$\zeta < 0$	$\zeta > 0$	$\zeta < 0$	$\zeta > 0$	$\zeta < 0$						
stability	on	off	on	off	on	off	on	off						
foliage	on	off	on	off	on	off	on	off						
UMBS														
46 m			690	903	712	736	588	1512	637	1178	708	1012	789	943
34 m			657	880	740	746	473	1484	499	1170	676	1006	767	931
MMSF														
46 m	669	614	538	369	259	571	356	975	311	619	635	1150	588	694
34 m	676	636	545	391	257	581	397	1015	295	666	685	1196	556	668

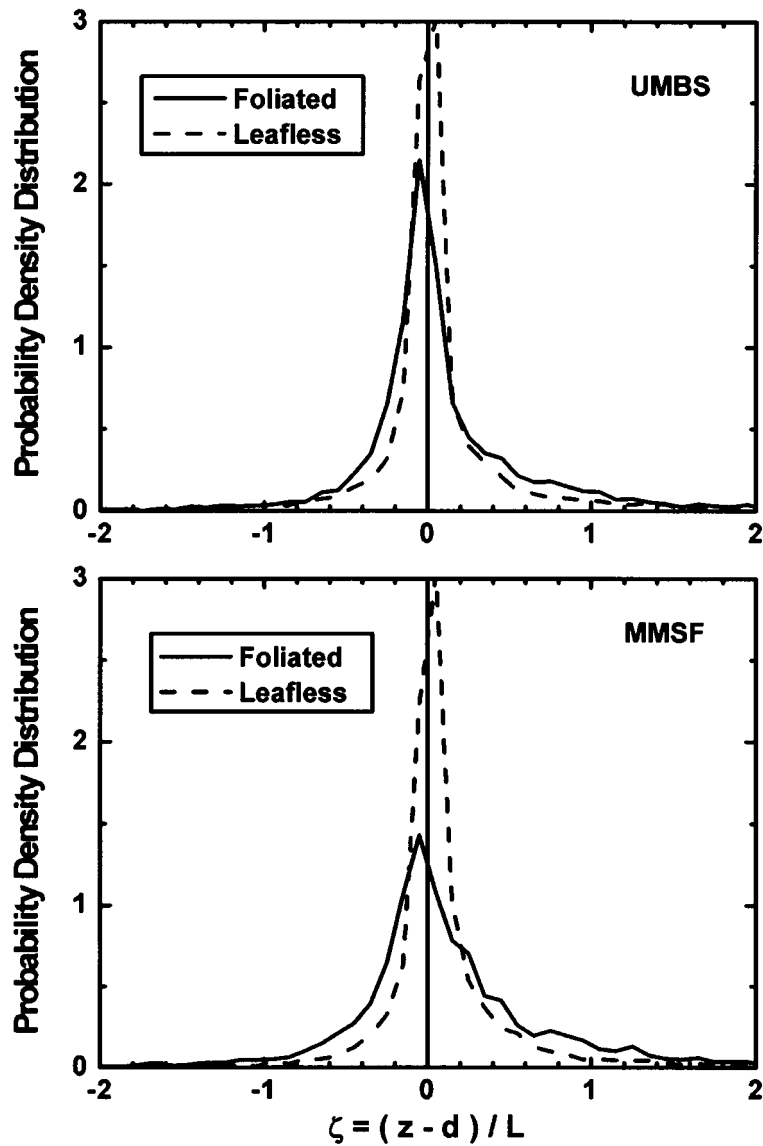


Figure 1. Probability distribution density function of the stability parameter ζ measured at the 46-m level at the UMBS (upper panel) and MMSF (lower panel) sites. Note that the integration of each curve over ζ equals 1.

3.1. THE SPECTRA OF VELOCITY COMPONENTS

In the inertial subrange, the spectrum, $S_u(n)$, of the longitudinal velocity (u) normalized by u_*^2 (u_* is the friction velocity) may be written as,

$$\begin{aligned}\frac{nS_u(n)}{u_*^2} &= \frac{\alpha}{(2\pi k)^{2/3}} \left[\frac{k(z-d)\epsilon}{u_*^2} \right]^{2/3} f^{-2/3} = \frac{\alpha}{(2\pi k)^{2/3}} \phi_\epsilon^{2/3}(\zeta) f^{-2/3} \\ &= a_u \phi_\epsilon^{2/3}(\zeta) f^{-2/3},\end{aligned}\quad (1)$$

where n is the natural frequency, $f = n(z-d)/U$ is a non-dimensional frequency, z is the measurement height, U is the local mean wind speed, k is the von Karman constant (0.4 in this study, 0.35 in Kaimal et al., 1972), α is a constant estimated to be about 0.5 and thus $a_u = 0.3$ (Kaimal et al., 1972), ϵ and ϕ_ϵ are the dimensional and non-dimensional dissipation rates of TKE, respectively.

Based on hot-wire measurement of ϵ , the Kansas experiment yielded (Wyngaard and Coté, 1971),

$$\phi_\epsilon^{2/3}(\zeta) = \begin{cases} 1 + 0.5(-\zeta)^{2/3}, & -2 \leq \zeta \leq 0 \\ 1 + 2.5\zeta^{3/5}, & 0 \leq \zeta \leq 2 \end{cases}. \quad (2)$$

Dividing Equation (1) by $\phi_\epsilon^{2/3}$, u spectra collapse into a single curve in the inertial subrange,

$$\frac{nS_u(n)}{u_*^2 \phi_\epsilon^{2/3}(\zeta)} = a_u f^{-2/3}, \quad (3)$$

and similarly, the inertial subrange spectra, $S_v(n)$ and $S_w(n)$, of the lateral (v) and vertical (w) velocity components can be collapsed into the same form,

$$\frac{nS_v(n)}{u_*^2 \phi_\epsilon^{2/3}(\zeta)} = a_v f^{-2/3}, \quad (4a)$$

$$\frac{nS_w(n)}{u_*^2 \phi_\epsilon^{2/3}(\zeta)} = a_w f^{-2/3}, \quad (4b)$$

and local isotropy predicts that in the inertial subrange, $S_v(n)$ and $S_w(n)$ are higher than $S_u(n)$ with a ratio of 4/3; thus, $a_v = a_w = 0.4$.

Using the Kansas u spectra, combined with either direct (hot-wire) measurements or indirect estimates (Equation (2)) of dissipation, Kaimal et al. (1972) estimated α to be about 0.5 ± 0.05 with no clear dependency on ζ . They also indicated that much higher values (up to 0.69) were reported by other studies; Höglström (1990) also reported a higher value (0.6) but dissipation was not directly measured in his experiment. Instead, he assumed that dissipation balances the shear production and the buoyancy term in the TKE budget, and used the empirical function of the non-dimensional shear derived from his experiment to estimate ϕ_ϵ . Note that Kaimal et al. (1972) used $k = 0.35$ in their calculation of α . If $k = 0.4$ is used, their estimate of α is reduced by about 10%.

In this study, we did not have either direct (hot-wire) measurement of ϵ or appropriate wind profile measurements to derive the empirical stability function for local non-dimensional shear production. Thus, we did not attempt to evaluate the values of α from our velocity spectral data. We can, however, use measured inertial subrange velocity spectra, together with Equations (3) and (4), to evaluate the products $a_u\phi_\epsilon^{2/3}(\zeta)$, $a_v\phi_\epsilon^{2/3}(\zeta)$ and $a_w\phi_\epsilon^{2/3}(\zeta)$, which were calculated at two frequencies $f = 4$ and 5 , while Kaimal et al. (1972) calculated at $f = 4$.

For neutral conditions ($\zeta = 0$), the values of $a_u\phi_\epsilon^{2/3}(0)$, $a_v\phi_\epsilon^{2/3}(0)$ and $a_w\phi_\epsilon^{2/3}(0)$ were estimated as ensemble averages over the range $-0.02 < \zeta < 0.02$ (Table II). In general, these products are larger at 46 m than at 34 m at the same site during the same season. This height difference is somewhat greater at UMBS (but smaller at MMSF) in the foliated season than the leafless season. The height differences are more similar between the two sites in the foliated season than in the leafless season. Seasonal changes in these products for the same height are much greater at MMSF; the products are greater in the foliated season and the seasonal change is greater at 34 m. At the UMBS site, the seasonal change is small at both heights; either negligible or opposite to the seasonal change at the MMSF site. Combining these products at both sites, they decrease with normalized height in the leafless season. However, such organized change is absent during the foliated season, possibly due in part to the difference in peak VAI between these two sites.

Variations in the ratio a_w/a_u with height and seasonal changes in VAI are similar to those of the above products (Table II). This is not the case for the ratio a_v/a_u . Both ratios are smaller than the $4/3$ value as predicted by isotropy; a_v/a_u ranges from 1.15 to 1.20 and a_w/a_u from 1.01 to 1.08. This result is in agreement with previous studies over forests (Anderson et al., 1986; Baldocchi and Meyers, 1988; Amiro, 1990), but differs from those of Kaimal et al. (1972) and Höögström (1990) over smoother surfaces. However, there are similarities in our velocity spectra with those of Kaimal et al. (1972). For example, in stable conditions, the ratios $S_v(n)/S_u(n)$ and $S_w(n)/S_u(n)$ reach their respective inertial range values at a higher f with increasing ζ (Figure 2). For the same ζ , $S_w(n)/S_u(n)$ reaches its inertial subrange value at a higher f than $S_v(n)/S_u(n)$, and even falls short at the most stable conditions. Such a transition of the ratios to their inertial range values is less organized in very unstable conditions, particularly for $S_v(n)/S_u(n)$.

The variations in the products $a_u\phi_\epsilon^{2/3}(0)$, $a_v\phi_\epsilon^{2/3}(0)$ and $a_w\phi_\epsilon^{2/3}(0)$ described above could be due in part to the variations in ϕ_ϵ with height. This may be discussed in terms of the TKE budget in the roughness layer over forest canopies. In a non-dimensional form, and assuming steady-state and horizontal homogeneity, the TKE budget equation, normalized by $k(z-d)/u_*^3$, reads,

$$\gamma(\phi_m - \zeta - \phi_t - \phi_p - \phi_\epsilon) = \frac{\gamma k(z-d)}{u_*} \frac{\partial U}{\partial z} - \gamma\zeta - \gamma\phi_t - \gamma\phi_p - \frac{\gamma k(z-d)\epsilon}{u_*^3} = 0, \quad (5)$$

TABLE II

Velocity spectra and their ratio in the inertial subrange in neutral conditions at the UMBS and MMSF sites.

z (m)	Foliage	$a_u \phi_\epsilon^{2/3}(0)$	$a_v \phi_\epsilon^{2/3}(0)$	$a_w \phi_\epsilon^{2/3}(0)$	a_v/a_u	a_w/a_u
UMBS						
46	on	0.314	0.372	0.335	1.18	1.07
46	off	0.312	0.375	0.338	1.20	1.08
34	on	0.284	0.339	0.288	1.19	1.01
34	off	0.295	0.346	0.298	1.17	1.01
MMSF						
46	on	0.361	0.418	0.386	1.16	1.07
46	off	0.298	0.347	0.309	1.16	1.04
34	on	0.329	0.377	0.340	1.15	1.03
34	off	0.239	0.278	0.241	1.16	1.01

where ϕ_m is the non-dimensional shear production, ϕ_t is the turbulent transport, and ϕ_p is the pressure transport. We added the eddy diffusivity enhancement factor $\gamma \geq 1$ to allow $\gamma \phi_m = 1$ regardless of the height in the roughness layer or the vegetation density (Garratt, 1992). Thus, we have $\phi_\epsilon = \phi_m - \zeta - \phi_t - \phi_p = \gamma^{-1} - \zeta - \phi_t - \phi_p$. Both wind-tunnel experiments (Raupach et al., 1986) and large-eddy simulation (Su et al., 1998) have shown that γ varies with height in the roughness sublayer; it could be influenced also by vegetation density but not much affected by stability (Garratt, 1992). The transport terms, ϕ_t and ϕ_p , also vary with height in the roughness sublayer (Kaimal and Finnigan, 1994; Dwyer et al., 1997), and could be influenced by canopy morphology. Thus, we can expect ϕ_ϵ to vary with height and VAI. Since $\gamma \geq 1$, and the transport terms appear as local sinks of TKE in the roughness sublayer above forest canopy (Kaimal and Finnigan, 1994; Dwyer et al., 1997), ϕ_ϵ is less than 1 in near-neutral conditions.

Assuming a_u does not change with stability, we can follow Kaimal et al. (1972) to evaluate $\phi_\epsilon^{2/3}(\zeta)$ as empirical functions of ζ . In doing so, we divided $a_u \phi_\epsilon^{2/3}(\zeta)$ by its neutral value $a_u \phi_\epsilon^{2/3}(0)$ so that the empirical functions equal 1 at $\zeta = 0$. In selecting the forms of such empirical functions, we considered both the TKE budget and published forms of empirical functions for other budget terms. For example, the form $\phi_m = (1 - \beta^- \zeta)^{-1/4}$ is often used for unstable conditions, while a linear form $\phi_m = 1 + \beta^+ \zeta$ has been observed for the stable surface layer (Stull, 1988; Sorbjan, 1989). Wyngaard and Coté (1971) found that ϕ_t is negligible in stable conditions, whereas in unstable conditions $\phi_t = -\zeta$. An empirical stability function for ϕ_p is generally lacking and thus not considered here.

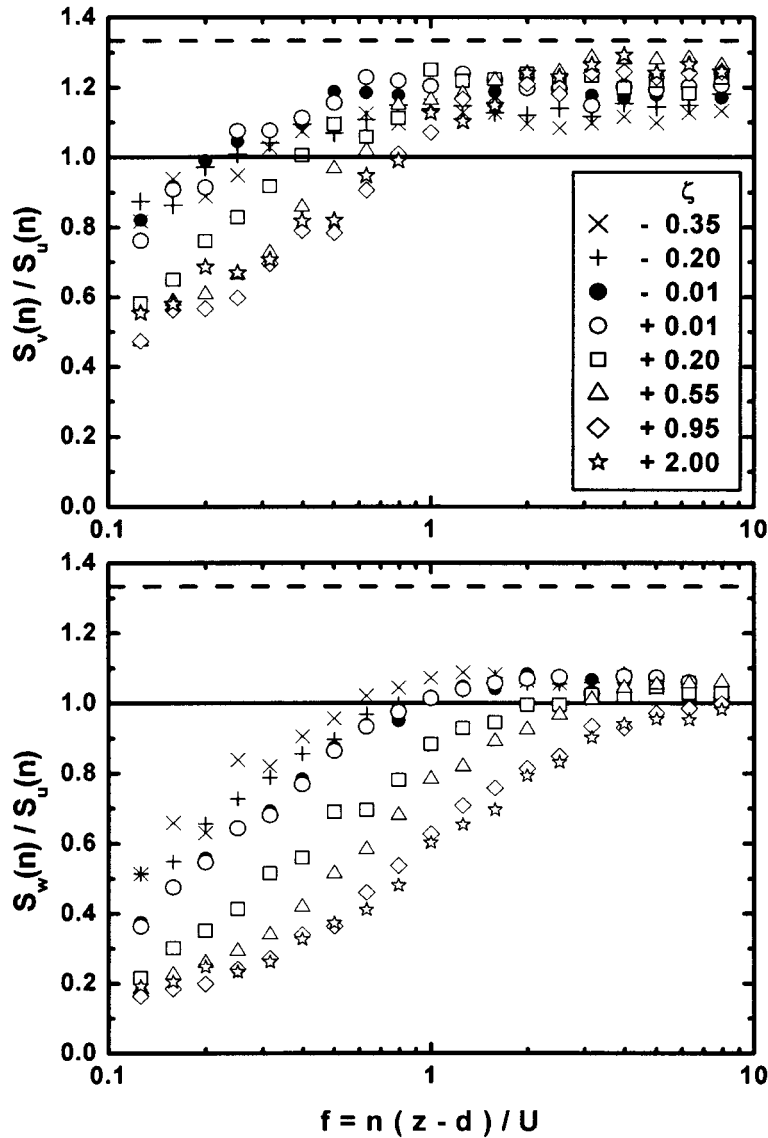


Figure 2. Ratios of v and w spectra to the u spectrum approaching constants in the inertial subrange but less than $4/3$ as predicted by isotropy. Data shown are for the foliated period at the 46-m level of the UMBS site.

Thus, for stable conditions, in addition to the form $\phi_\epsilon^{2/3} = 1 + b_1^+ \zeta^{3/5}$ in Equation (2), the form $\phi_\epsilon^{2/3} = 1 + b_2^+ \zeta^{2/3}$ was also used (Garratt, 1972; Wyngaard, 1975; Kaimal and Finnigan, 1994). However, we found that the former yielded a better fit to our data, particularly for $0 < \zeta < 0.5$ (not shown for the sake of brevity). The coefficient b_2^+ varies between different studies, from 3.7 in Garratt (1972), 4 in

TABLE III

Empirical coefficients in the stability functions (non-dimensional dissipation) used to collapse velocity spectra in the inertial subrange (Equation (6)) at the UMBS and MMSF sites.

z (m)	Foliage	b_1^+	b_2^+	b^-	c^-
UMBS					
46	on	1.50	2.94	31.1	0.94
46	off	1.56	3.07	35.5	0.64
34	on	2.04	4.26	25.5	1.10
34	off	1.88	3.86	117.8	1.10
MMSF					
46	on	1.28	2.42	30.2	0.59
46	off	1.95	4.05	43.5	0.81
34	on	1.25	2.30	129.0	1.25
34	off	2.39	5.19	75.7	1.43

Wyngaard (1975), to 5 in Kaimal and Finnigan (1994). Note that the Kansas data yielded $b_2^+ = 2b_1^+$ (Kaimal et al., 1972; Kaimal and Finnigan, 1994).

For unstable conditions, we observed that $\phi_\epsilon^{2/3}(\zeta)/\phi_\epsilon^{2/3}(0)$ first decreases from 1 at $\zeta = 0$ to a minimum approximately at $\zeta = -0.25$ before starting to increase with more negative ζ (Figure 3). This feature cannot be described by Equation (2). We found that the decrease can be described well by the known form $\phi_m = (1 - \beta^- \zeta)^{-1/4}$ as in Garratt (1972), accounting for shear production of TKE in this stability range. Högström (1990) used the form $\phi_\epsilon = 1.24[(1 - 19\zeta)^{-1/4} - \zeta]$ and the factor 1.24 indicated that they found the dissipation was greater than the shear and buoyancy productions in unstable conditions.

With the above considerations, we chose the following functions to fit our data,

$$\frac{\phi_\epsilon^{2/3}(\zeta)}{\phi_\epsilon^{2/3}(0)} = \begin{cases} [(1 - b^- \zeta)^{-1/4} - c^- \zeta]^{2/3}, & -2 \leq \zeta \leq 0 \\ 1 + b_1^+ \zeta^{3/5} \text{ or } (1 + b_2^+)^{2/3}, & 0 \leq \zeta \leq 2 \end{cases}, \quad (6)$$

where we added the coefficient c^- to the buoyancy term ζ to take into account the fact that c^- is about 0.5 in very unstable conditions (corresponding to the unstable limit of Equation (2)) and that the transport term may be proportional to ζ in unstable conditions (Wyngaard and Coté, 1971). This added freedom also improved the non-linear fit compared to setting $c^- = 1$ to our data (not shown for the sake of brevity). The non-linear fit results are given in Table III and shown in Figure 3 in comparison with Equation (2).

For stable conditions, the coefficient b_2^+ (from 2.30 to 5.19) is about twice b_1^+ (from 1.25 to 2.39) for the same height during the same season. This is similar

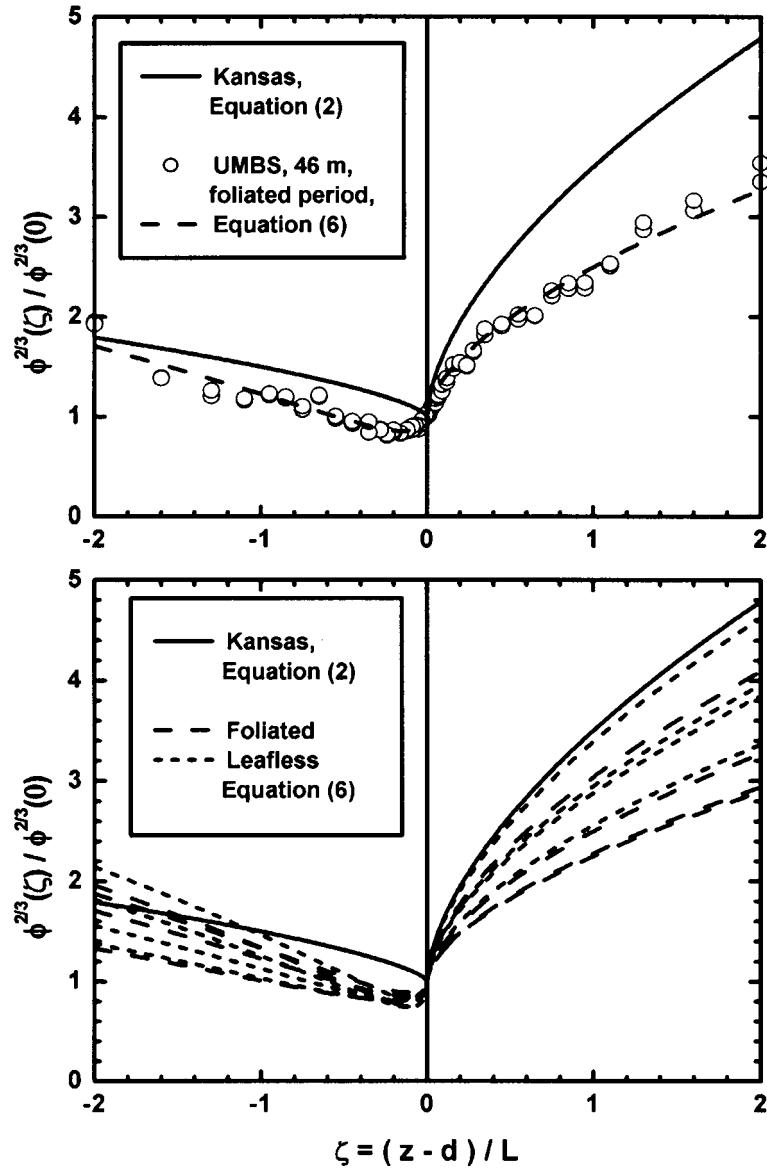


Figure 3. Comparison of stability function of $\phi_\epsilon^{2/3}(\zeta)/\phi_\epsilon^{2/3}(0)$. Upper panel: Points and dashed curves (Equation (6)) are based on spectra measured at the 46-m level at the UMBS site during the summer. Lower panel: Long dashed curves (foliated season) and short dashed (leafless season) are fits to Equation (6) using measured spectra at all four heights at both sites to illustrate the range of variations and seasonal differences. The solid curves in both panels are from Equation (2) after Kaimal et al. (1972). For the stable conditions, all the curves shown are based on the formula $\phi_\epsilon^{2/3} = 1 + b_1^+ \zeta^{3/5}$.

to the Kansas data when the same two functions were used (Kaimal et al., 1972; Kaimal and Finnigan, 1994). In comparison with the products $a_u\phi_\epsilon^{2/3}(0)$, $a_v\phi_\epsilon^{2/3}(0)$ and $a_w\phi_\epsilon^{2/3}(0)$ (Table II), one difference is that b_2^+ and b_1^+ are generally greater at the lower level at the same site during the same season. However, their variations with height and seasonal change in VAI are similar. Variations with height are less at MMSF than at UMBS during the foliated season, but more similar between the two sites in the leafless period. Seasonal differences for the same height are the least (negligible) at the 46-m level of the UMBS site and the greatest (factor of 2) at the 34-m level of the MMSF site. Again, this could be due to the difference in normalized measurement height as well as greater peak VAI at the MMSF site. In the foliated season, b_2^+ and b_1^+ are much smaller than those of the Kansas results, particularly at the MMSF site, indicating that ϕ_ϵ in the roughness sublayer over forest canopies increases with ζ less rapidly than is observed in the stable surface layer over a much less rough surface. The differences in b_2^+ and b_1^+ from the Kansas results are generally reduced in the leafless season (Figure 3).

In unstable conditions, the initial decrease in ϕ_ϵ from $\zeta = 0$ to $\zeta = -0.25$ is consistent for all heights at both sites regardless of seasonality in VAI (Figure 3). For $\zeta < -0.25$, ϕ_ϵ generally increases more rapidly with increasingly negative ζ than observed in the Kansas experiment. At both sites, seasonal changes in b^- (related to shear production) are greater at 34 m, but seasonal changes in c^- (related to buoyancy production) are greater at the 46-m level. However, variations in b^- and c^- with height and season are not as clearly organized as in $a_u\phi_\epsilon^{2/3}(0)$, $a_v\phi_\epsilon^{2/3}(0)$, $a_w\phi_\epsilon^{2/3}(0)$, b_2^+ and b_1^+ .

Normalized velocity spectra (Figure 4) illustrate many characteristics similar to those in Kaimal et al. (1972). The spectra fall together in the inertial subrange, where they follow the $-2/3$ slope quite well. The separations according to ζ are illustrated by the orderly shift of the spectral peaks and the lower frequency roll-off following a slope of about $+1$ in the direction of decreased f for ζ from $+0.95$ to -0.20 . In stable conditions, peak frequencies are highest for w spectra and least for u spectra for the same stability. Spectra for $\zeta < -0.20$ in the lowest frequencies are clustered, and spectra in the range $+0.95 < \zeta < +2$ overlap with the spectra of $\zeta = +0.95$; they are thus not shown for clarity.

3.2. THE COSPECTRA OF VERTICAL MOMENTUM AND SENSIBLE HEAT FLUXES

Similar to the velocity spectra, dimensional analysis (Wyngaard and Coté, 1972) predicted that the inertial subrange cospectrum, $\text{Co}_{uw}(n)$, of the vertical momentum flux, has the form,

$$\frac{n\text{Co}_{uw}(n)}{\overline{u'w'}} = \frac{\alpha_{uw}}{(2\pi k)^{4/3}} \phi_m(\zeta) \phi_\epsilon^{1/3}(\zeta) f^{-4/3}, \quad (7)$$

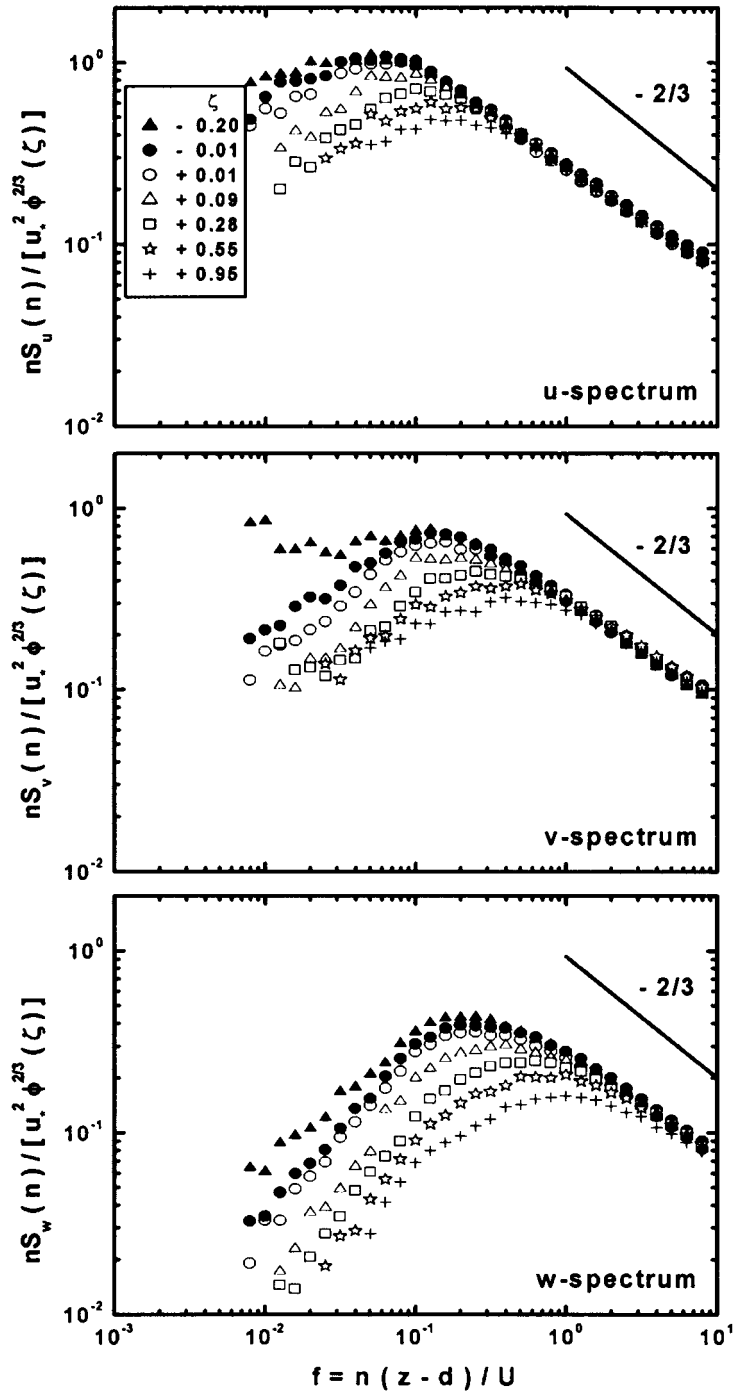


Figure 4. Normalized velocity spectra. Data shown are for the foliated period at the 46-m level of the UMBS site.

and the cospectrum, $\text{Co}_{w\theta}(n)$, of the vertical sensible heat flux is in the form,

$$\frac{n\text{Co}_{w\theta}(n)}{w'\theta'} = \frac{\alpha_{w\theta}}{(2\pi k)^{4/3}} \phi_h(\zeta) \phi_\epsilon^{1/3}(\zeta) f^{-4/3}, \quad (8)$$

where ϕ_h is the non-dimensional temperature gradient. Using local free convection scaling, Wyngaard and Coté (1972) predicted that α_{uw} and $\alpha_{w\theta}$ approach constant values in the free convection limit. They also evaluated the behaviour of α_{uw} and $\alpha_{w\theta}$ with stability, using observed formulae for ϕ_h and ϕ_ϵ . This was combined with an observed empirical function of ϕ_m for $\zeta < -0.5$ to predict that the right-hand sides of Equations (7) and (8) become $a_{uw} f^{-4/3}$ and $a_{w\theta} f^{-4/3}$, respectively, for unstable conditions, with $a_{uw} = 0.043$ and $a_{w\theta} = 0.138$. Kaimal et al. (1972) used slightly higher values $a_{uw} = 0.048$ and $a_{w\theta} = 0.140$.

Using local z-less scaling, Wyngaard and Coté (1972) predicted that under very stable conditions,

$$\frac{n\text{Co}_{uw}(n)}{u'w'} \propto \frac{n\text{Co}_{w\theta}(n)}{w'\theta'} \propto \zeta^{4/3}, \quad (9)$$

which can be seen easily from Equations (7) and (8), and that ϕ_m , ϕ_h and ϕ_ϵ are all proportional to ζ under very stable conditions, as they observed in the surface layer.

Kaimal et al. (1972) wrote Equation (7) as

$$\frac{n\text{Co}_{uw}(n)}{u'w'} = a_{uw} G_{uw}(\zeta) f^{-4/3}, \quad (10)$$

and Equation (8) as,

$$\frac{n\text{Co}_{w\theta}(n)}{w'\theta'} = a_{w\theta} G_{w\theta}(\zeta) f^{-4/3}, \quad (11)$$

where they used linear forms for $G_{uw}(\zeta)$ and $G_{w\theta}(\zeta)$ in stable conditions with the linear coefficients estimated empirically from measured cospectra in the inertial range at the non-dimensional frequency $f = 4$,

$$G_{uw}(\zeta) = \begin{cases} 1, & -2 \leq \zeta \leq 0 \\ 1 + 7.9\zeta, & 0 \leq \zeta \leq 2 \end{cases}, \quad (12)$$

$$G_{w\theta}(\zeta) = \begin{cases} 1, & -2 \leq \zeta \leq 0 \\ 1 + 6.4\zeta, & 0 \leq \zeta \leq 2 \end{cases}. \quad (13)$$

In the usual range of ζ in stable conditions (e.g., $\zeta < 0.5$ in Figure 1), the non-linearity (Equation (9)) in $G_{uw}(\zeta)$ and $G_{w\theta}(\zeta)$ may be small (Wyngaard and Coté, 1972).

TABLE IV

Empirical coefficients in the stability functions used to collapse co-spectra in the inertial subrange (Equations (14) and (15)) at the UMBS and MMSF sites.

z (m)	Foliage	a_{uw}	$a_{w\theta}$	b_{uw}	c_{uw}	$b_{w\theta}$	$c_{w\theta}$
UMBS							
46	on	0.052	0.151	4.65	0.72	2.68	0.45
46	off	0.041	0.136	5.73	0.69	3.15	0.44
34	on	0.028	0.113	6.17	0.59	3.21	0.36
34	off	0.025	0.107	7.13	0.71	3.77	0.43
MMSF							
46	on	0.055	0.160	4.13	0.49	2.27	0.28
46	off	0.042	0.110	7.16	0.62	4.24	0.36
34	on	0.045	0.130	4.42	0.50	2.10	0.26
34	off	0.024	0.090	13.02	0.54	5.41	0.34

Using measured inertial subrange cospectra at $f = 4$ and 5 , we estimated the values of a_{uw} and $a_{w\theta}$ as ensemble averages in the range $-0.5 < \zeta < -0.02$ (Table IV) as $\text{Co}_{uw}(n)$ and $\text{Co}_{w\theta}(n)$ are very small in the inertial subrange in very unstable and near-neutral conditions, respectively, where the measurement error could be large. In general, a_{uw} and $a_{w\theta}$ are greater at the higher level of both sites. They are also larger for the same height during the foliated period. Seasonal differences for the same height are also greater at the MMSF site, as expected from the greater peak VAI. The variations in a_{uw} and $a_{w\theta}$ presented here, and their deviations from the Kansas data (Wyngaard and Coté, 1972), could be due to the differences and variations in ϕ_m , ϕ_h and ϕ_ϵ over forest canopies of different morphology. Although we did not have direct measurements of local ϕ_m and ϕ_h and other supporting data to analyze the behaviour of α_{uw} and $\alpha_{w\theta}$ from the neutral to the unstable limit, our earlier analysis of $\phi_\epsilon^{2/3}$ (Figure 3, Tables II and III) showed that ϕ_ϵ over forests follows a different functional form from the Kansas results in unstable conditions, particularly for $-0.5 < \zeta < 0$.

In stable conditions, we found that the linear Equations (12) and (13) hold up only when $\zeta < 0.5$ (Figure 5). The stability functions $G_{uw}(\zeta)$ and $G_{w\theta}(\zeta)$ increase less rapidly with ζ than the linear prediction when $\zeta > 0.5$. Thus, we used the following non-linear form,

$$G_{uw}(\zeta) = \begin{cases} 1, & -2 \leq \zeta \leq 0 \\ 1 + b_{uw}\zeta^{c_{uw}}, & 0 \leq \zeta \leq 2 \end{cases}, \quad (14)$$

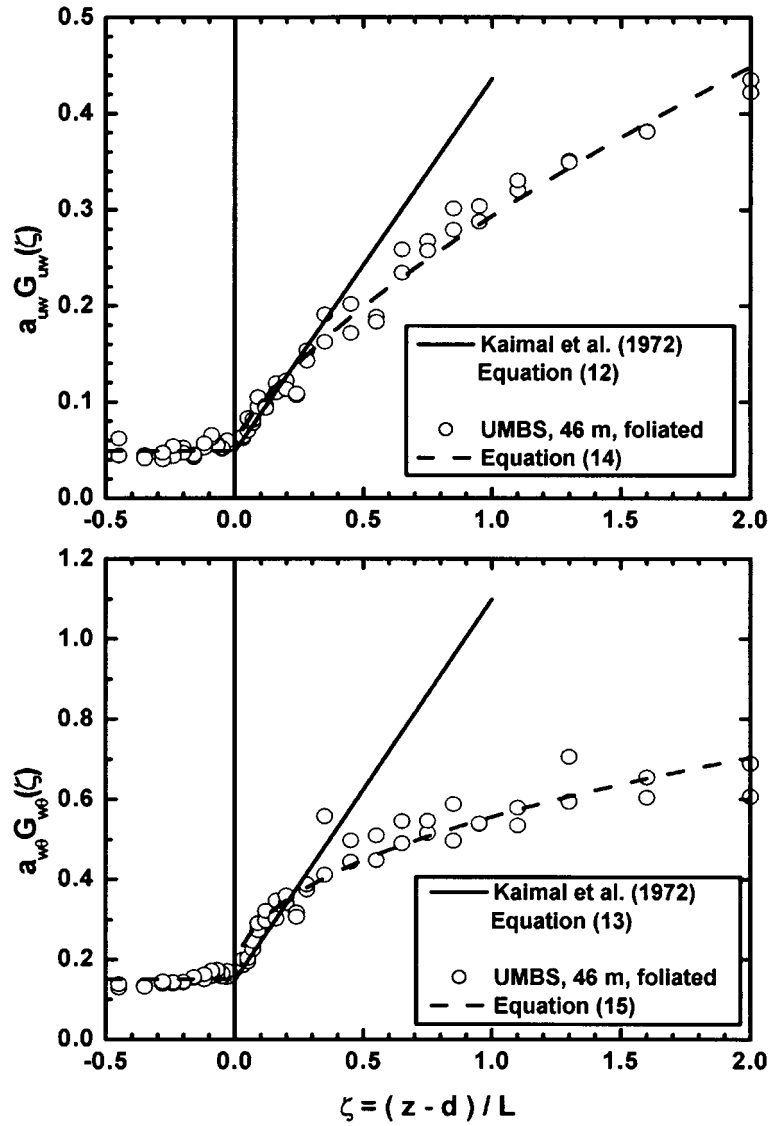


Figure 5. Estimates of $a_{uw}G_{uw}(\zeta)$ (upper panel) and $a_{w\theta}G_{w\theta}(\zeta)$ (lower panel) using measured cospectra at $f = 4$ and 5 , in comparison with Kaimal et al. (1972). Points and dashed curves are estimates for the foliated period at the 46-m level of the UMBS site.

and

$$G_{w\theta}(\zeta) = \begin{cases} 1, & -2 \leq \zeta \leq 0 \\ 1 + b_{w\theta}\zeta^{c_{w\theta}}, & 0 \leq \zeta \leq 2 \end{cases}, \quad (15)$$

where the coefficients b_{uw} , c_{uw} , $b_{w\theta}$ and $c_{w\theta}$ were estimated from measured inertial subrange cospectra at $f = 4$ and 5 (Table IV). In general, b_{uw} (from 4.13 to 13.02)

is greater than $b_{w\theta}$ (from 2.10 to 5.41) by a factor of about 2, more than the relative difference in respective linear-fit coefficients in Equations (12) and (13). Also, c_{uw} (from 0.49 to 0.72) is greater than $c_{w\theta}$ (from 0.26 to 0.45). Thus, $G_{uw}(\theta)$ increases more rapidly with ζ than $G_{w\theta}(\zeta)$ in stable conditions. The variations of b_{uw} , c_{uw} , $b_{w\theta}$ and $c_{w\theta}$ with height and VAI are generally opposite to that of a_{uw} and $a_{w\theta}$. For example, they are generally greater closer to the canopy and during the leaf-off periods. Seasonal differences are again greater at the MMSF site. For very stable conditions, our estimated values of c_{uw} and $c_{w\theta}$ (less than 1) further deviate from 4/3 as predicted by Wyngaard and Coté (1972) than the linear prediction. Lack of supporting measurements of ϕ_m and ϕ_h under stable conditions prevented an examination of how these functions over forest canopies in the roughness layer may differ from those used in the analysis of Wyngaard and Coté (1972).

As expected, normalized cospectra collapse in the inertial subrange where they follow a slope close to $-4/3$, and which started at a higher f for $\text{Co}_{w\theta}(n)$ than for $\text{Co}_{uw}(n)$ (Figure 6). We also included a_{uw} and $a_{w\theta}$ in the normalization so that $\text{Co}_{w\theta}(n)$ and $\text{Co}_{uw}(n)$ would be equal at the same f in the inertial range. This would allow a better comparison between $\text{Co}_{w\theta}(n)$ and $\text{Co}_{uw}(n)$ for the same height, as well as $\text{Co}_{w\theta}(n)$ or $\text{Co}_{uw}(n)$ at all heights at both sites since a_{uw} , $a_{w\theta}$, b_{uw} , c_{uw} , $b_{w\theta}$ and $c_{w\theta}$ all vary with height and VAI. For example, as indicated by Kaimal et al. (1972), in the lower frequency range (f less than the peak frequency), normalized heat flux cospectral densities in unstable conditions are smaller than those of momentum flux, and thus larger eddies are relatively more efficient in transporting momentum than scalar in the vertical direction.

3.3. EMPIRICAL COSPECTRA MODELS

Empirical cospectral formulae from Kaimal et al. (1972) have often been used in estimates of frequency loss of measured fluxes in the surface layer (Moore, 1986; Ribmann and Tetzlaff, 1994; Eugster and Senn, 1995; Horst, 1997; Massman, 2000). Here we examine how these cospectral models fit our observations over forest.

3.3.1. Neutral and Unstable Conditions

For an unstable surface layer, Kaimal and Finnigan (1994) used the cospectral formulae in near-neutral conditions from Kaimal et al. (1972) because unstable cospectra in the low frequency end are clustered –

$$\frac{n\text{Co}_{uw}(n)}{u'w'} = \frac{\beta_{-1}^{uw} f}{(1 + \beta_{-2}^{uw} f)^{7/3}}, \quad (16)$$

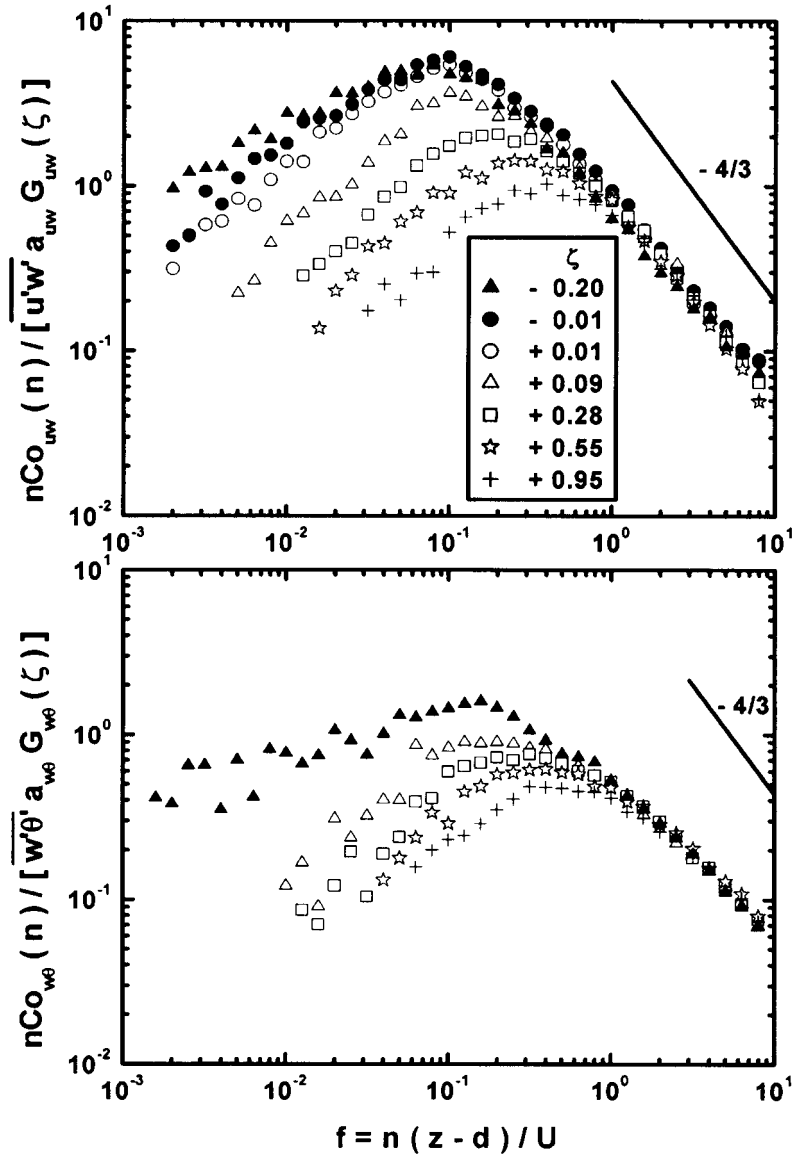


Figure 6. Normalized cospectra. Data shown are for the foliated period at the 46-m level of the UMBS site.

where $\beta_{-1}^{uw} = 12$, $\beta_{-2}^{uw} = 9.6$, and,

$$\frac{nCo_{w\theta}(n)}{w'\theta'} = \left\{ \begin{array}{ll} \frac{\beta_{-1}^{w\theta} f}{(1 + \beta_{-2}^{w\theta} f)^{7/4}}, & f \leq 1 \\ \frac{\beta_{-3}^{w\theta} f}{(1 + \beta_{-4}^{w\theta} f)^{7/3}}, & f \geq 1 \end{array} \right\}, \tag{17}$$

where $\beta_{-1}^{w\theta} = 11$, $\beta_{-2}^{w\theta} = 13.3$, $\beta_{-3}^{w\theta} = 4$ and $\beta_{-4}^{w\theta} = 3.8$.

Sakai et al. (2001) used a single form to fit both momentum and scalar cospectra in the roughness layer over forests in convective conditions, viz.

$$\frac{n\text{Co}_{xy}(n)}{x'y'} = \frac{\beta_{-5}^{xy} f}{1 + (\beta_{-6}^{xy} f)^{7/3}}, \quad (18)$$

where $\beta_{-5}^{uw} = 8.5$, $\beta_{-6}^{uw} = 12.4$ and $\beta_{-5}^{w\theta} = 7.6$, $\beta_{-6}^{w\theta} = 11.5$ in the foliated season at Harvard Forest, with slightly smaller values during the leaf-off periods. The eddy-covariance system at the Harvard Forest site is at a height of 30 m, or $1.3h_C$, which is at a normalized height very close to the 34-m level at the MMSF site.

As discussed at the end of Section 3.2, larger eddies are relatively more efficient in the transport of momentum, while smaller eddies are relatively more efficient in transporting heat. This feature is clearly shown in Figure 7 (top panel), and consistent for all heights and seasons (even though not shown here for the sake of brevity). Thus, empirical cospectral models for vertical momentum and scalar fluxes should be different in unstable conditions. In addition, we used cospectra in the frequency band $0.01 < f < 10$ to fit the empirical cospectral formulae. This band covers the most important turbulent scales, about a decade from the peak frequency in the lowest frequency end, and about a decade of inertial subrange at the highest frequency end, as shown in both Figure 6 and in Kaimal et al. (1972) and Sakai et al. (2001). This choice avoids the greater variability in the cospectra when $f < 0.01$ due to inadequate sampling, red noise, mesoscale influence, natural variability. Above $f = 10$, measurement errors could be relatively large as the cospectral densities are small.

For the normalized momentum cospectra, Equation (16) generally fits our data better than Equation (18) (middle panel in Figure 7, and Table V). The functional form of Equation (18) fits the more sharply peaked cospectra better than Equation (16), as reported in Sakai et al. (2001). This difference was also shown in Horst (1997) where a form similar to Equation (18) was used for all stability conditions, except that he used an exponent of 2 instead of 7/3 to make the relationship more amenable to analytical treatment. Thus, we also used the following formulae, a slight modification from Equation (17) for $f \leq 1$,

$$\frac{n\text{Co}_{w\theta}(n)}{w'\theta'} = \left\{ \begin{array}{ll} \frac{\beta_{-7}^{w\theta} f}{1 + (\beta_{-8}^{w\theta} f)^{7/4}}, & f \leq 1 \\ \frac{\beta_{-3}^{w\theta} f}{(1 + \beta_{-4}^{w\theta} f)^{7/3}}, & f \geq 1 \end{array} \right\}. \quad (19)$$

This form fits our normalized vertical heat flux cospectra in the lower frequency ($f \leq 1$) band better at the 34-m level during the foliated season at both sites (Table V). This may confirm the observation of Sakai et al. (2001) that $\text{Co}_{w\theta}(n)$ close to the canopy over forest is more sharply peaked than those in Kaimal et al. (1972),

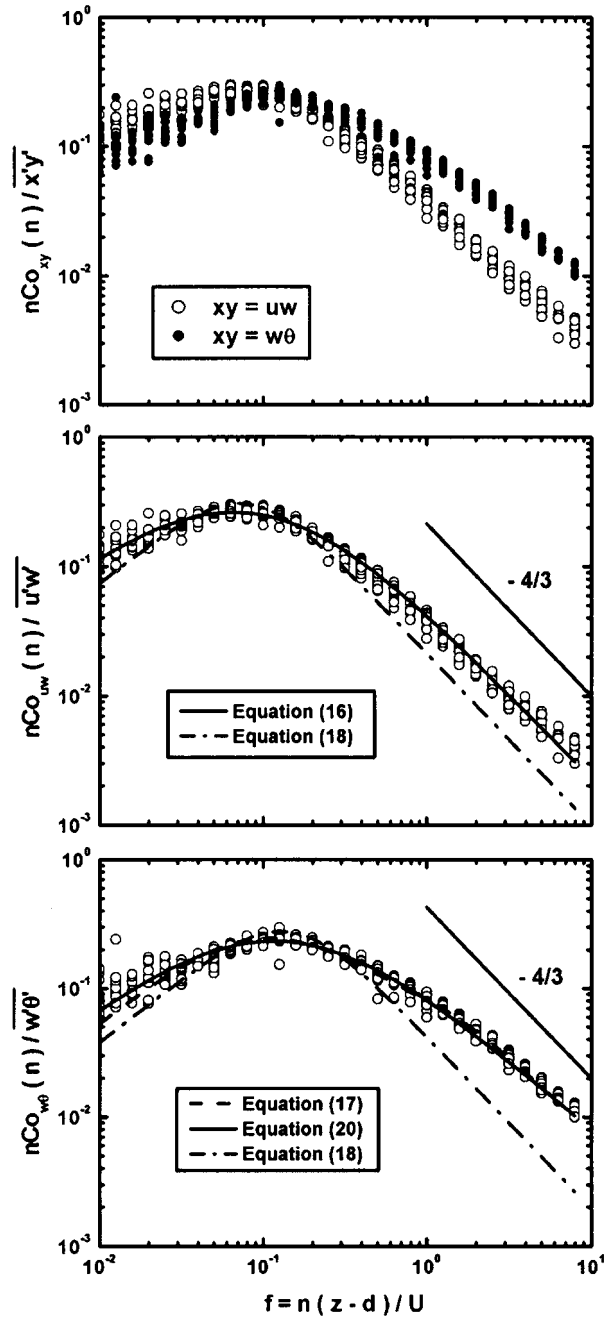


Figure 7. Cospectral models for neutral and unstable conditions. Top panel: the difference between the cospectra for the vertical momentum and sensible heat fluxes. Middle panel: Cospectra of the vertical momentum fluxes. Bottom panel: Cospectra of the vertical sensible heat fluxes. Points (measurements) and curves (models) are for the foliated period at the 46-m level of the UMBS site.

TABLE V

Empirical coefficients in the model cospectra in neutral and unstable conditions (Equations (16) to (20)) are given in the upper half of the table. The root-mean-square-error (RMSE) and coefficient of determination (R^2) of the non-linear least square fit are given in the lower half of the table.

z (m)	Foliage	β_{-1}^{uw}	β_{-2}^{uw}	β_{-5}^{uw}	β_{-6}^{uw}	$\beta_{-1}^{w\theta}$	$\beta_{-2}^{w\theta}$	$\beta_{-3}^{w\theta}$	$\beta_{-4}^{w\theta}$	$\beta_{-5}^{w\theta}$	$\beta_{-6}^{w\theta}$	$\beta_{-7}^{w\theta}$	$\beta_{-8}^{w\theta}$	$\beta_{-9}^{w\theta}$	$\beta_{-10}^{w\theta}$
UMBS															
46	on	14.8	11.4	7.4	12.3	9.2	12.5	1.8	2.7	3.8	6.9	5.4	11.0	8.2	8.9
46	off	17.1	13.2	8.5	14.0	10.8	15.1	1.9	2.9	4.2	7.9	6.3	13.2	9.5	10.5
34	on	17.1	12.6	8.5	13.3	11.5	14.8	1.7	3.1	4.8	8.2	6.7	12.9	10.4	10.6
34	off	20.0	15.1	9.8	15.8	13.2	17.7	1.7	3.2	5.2	9.3	7.5	15.2	11.6	12.4
MMSF															
46	on	13.0	10.1	6.6	10.8	9.6	13.5	0.9	1.8	4.0	7.4	5.6	11.9	8.5	9.6
46	off	16.7	13.0	8.3	13.8	12.1	16.7	2.0	3.3	4.6	8.6	6.9	14.4	10.6	11.6
34	on	13.8	10.1	7.1	10.9	10.9	14.3	1.0	2.3	4.6	8.0	6.4	12.6	9.8	10.3
34	off	18.8	14.3	9.2	15.0	14.4	19.4	1.3	3.1	5.5	10.0	8.1	16.5	12.6	13.5
z (m)	Foliage	RMSE	R^2	RMSE	R^2	RMSE	R^2	RMSE	R^2	RMSE	R^2	RMSE	R^2	RMSE	R^2
UMBS															
46	on	0.018	0.967	0.029	0.911	0.025	0.809	0.005	0.964	0.036	0.768	0.027	0.782	0.020	0.927
46	off	0.019	0.962	0.033	0.882	0.022	0.817	0.005	0.960	0.041	0.675	0.029	0.683	0.019	0.927
34	on	0.023	0.955	0.026	0.940	0.030	0.824	0.003	0.984	0.027	0.904	0.024	0.894	0.022	0.937
34	off	0.021	0.959	0.031	0.908	0.027	0.824	0.004	0.957	0.035	0.812	0.027	0.819	0.021	0.934
MMSF															
46	on	0.021	0.954	0.028	0.917	0.039	0.659	0.009	0.880	0.040	0.731	0.038	0.677	0.032	0.835
46	off	0.020	0.957	0.033	0.885	0.030	0.737	0.005	0.942	0.042	0.703	0.034	0.656	0.025	0.893
34	on	0.025	0.944	0.022	0.956	0.032	0.809	0.003	0.980	0.026	0.905	0.024	0.890	0.023	0.927
34	off	0.019	0.967	0.026	0.934	0.029	0.815	0.002	0.980	0.035	0.821	0.029	0.815	0.022	0.928

as the best fit using Equation (18) was also obtained when applied to measured $\text{Co}_{w\theta}(n)$ at the 34-m level at both sites during the foliated period (Table V).

Moreover, we found that the following simpler one-part form, similar to that of Horst (1997) in that the exponent is 2, yielded much better fits than Equation (18) for all heights and seasons (Table V):

$$\frac{n\text{Co}_{w\theta}(n)}{w'\theta'} = \frac{\beta_{-9}^{w\theta} f}{(1 + \beta_{-10}^{w\theta} f)^2}. \quad (20)$$

This indicates that our observed $\text{Co}_{w\theta}(n)$ is not as sharply peaked as reported by Sakai et al. (2001) (bottom panel in Figure 7), including those at the 34-m level at the MMSF site in the foliated season (Table V), which as noted above is at a similar normalized height as the observations at Harvard Forest used by Sakai et al. (2001).

The coefficients β_{-1}^{uw} and β_{-2}^{uw} are generally larger, and $\beta_{-3}^{w\theta}$ and $\beta_{-4}^{w\theta}$ are smaller, than respective values in Kaimal et al. (1972). This is not always the case for $\beta_{-1}^{w\theta}$ and $\beta_{-2}^{w\theta}$. All the coefficients in Table V are generally greater at the lower level in the same season. Seasonal differences for the same height are greater at the MMSF site, which again could be due to the higher peak VAI, and the greater mean canopy height.

3.3.2. Stable Conditions

In the stable surface layer, the cospectra for both momentum and sensible heat fluxes are described by the same formula in Kaimal et al. (1972):

$$\frac{n\text{Co}_{xy}(n)}{x'y'} = \frac{\beta_{+1}^{xy} (f/f_0)}{1 + \beta_{+2}^{xy} (f/f_0)^{2.1}}, \quad (21)$$

where $\beta_{+1}^{xy} = 0.88$ and $\beta_{+2}^{xy} = 1.5$ for both $xy = uw$ and $xy = w\theta$, and f_0 is defined by the intercept between the straight line extended from the $-4/3$ slope in the inertial subrange and the $n\text{Co}_{xy}(n)/x'y' = 1$ line. Thus, from Equations (10) and (11), we have,

$$f_0 = [a_{xy} G_{xy}(\zeta)]^{3/4}. \quad (22)$$

In general, Equation (21) fits measured $\text{Co}_{uw}(n)$ quite well, but for measured $\text{Co}_{w\theta}(n)$, the following form yielded a better fit (Figure 8, and Table VI),

$$\frac{n\text{Co}_{w\theta}(n)}{w'\theta'} = \frac{\beta_{+3}^{w\theta} (f/f_0)}{1 + \beta_{+4}^{w\theta} (f/f_0)^{2.1}}. \quad (23)$$

This form fits less sharply peaked cospectra better, as discussed earlier.

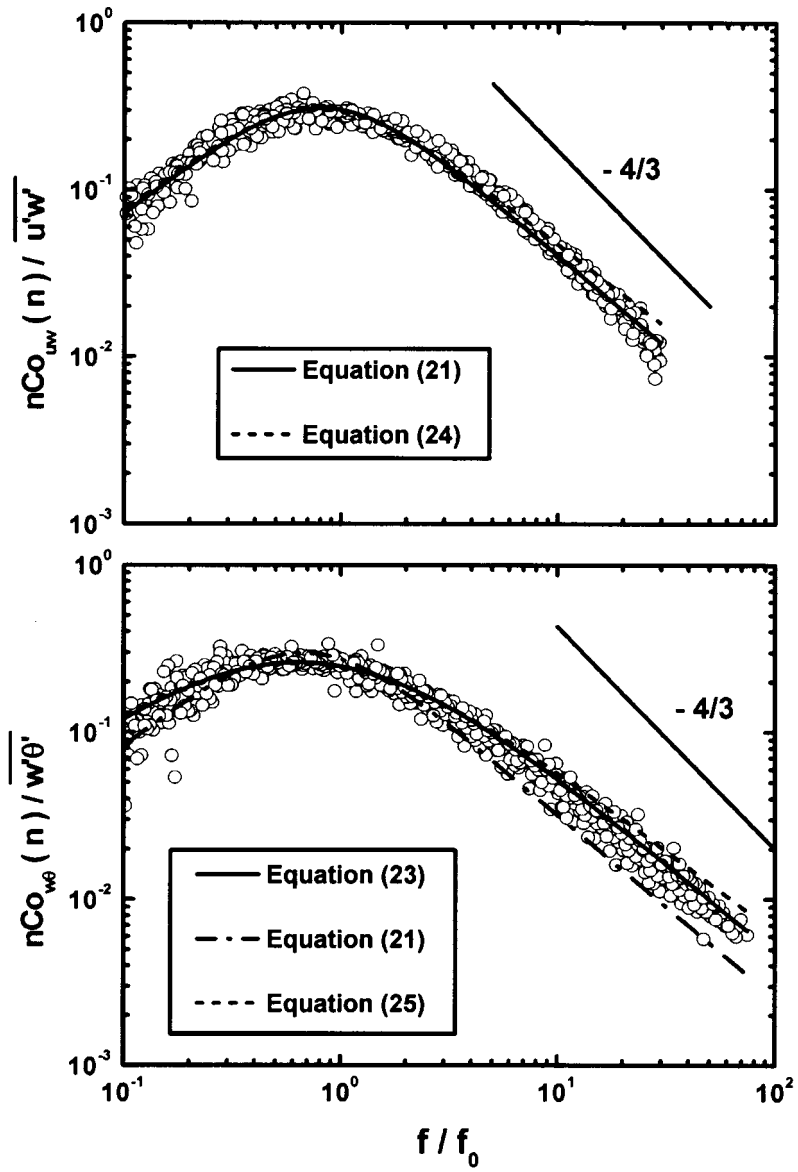


Figure 8. Cospectral models for stable conditions. Upper panel: cospectra of the vertical momentum fluxes. Lower panel: Cospectra of the vertical sensible heat fluxes. Points (measurements) and curves (models) are for the foliated period at the 46-m level of the UMBS site.

TABLE VI

Similar to Table V but for empirical coefficients in the model cospectra in stable conditions (Equations (21) to (25)).

z (m)	Foliage	β_{+1}^{uw}	β_{+2}^{uw}	β_{+5}^{uw}	β_{+6}^{uw}	$\beta_{+1}^{w\theta}$	$\beta_{+2}^{w\theta}$	$\beta_{+3}^{w\theta}$	$\beta_{+4}^{w\theta}$	$\beta_{+7}^{w\theta}$	$\beta_{+8}^{w\theta}$
UMBS											
46	on	0.73	1.44	0.77	1.63	0.84	2.08	1.58	1.42	1.65	1.61
46	off	0.69	1.20	0.73	1.37	0.90	2.17	1.69	1.45	1.77	1.65
34	on	0.76	1.34	0.80	1.51	1.17	3.83	2.20	1.88	2.31	2.13
34	off	0.70	1.03	0.73	1.19	1.08	3.08	2.04	1.71	2.14	1.94
MMSF											
46	on	0.86	1.85	0.91	2.07	1.03	2.79	1.95	1.64	2.04	1.86
46	off	0.88	1.89	0.93	2.12	0.97	2.69	1.83	1.60	1.92	1.81
34	on	0.94	1.97	0.98	2.18	1.49	5.60	2.76	2.23	2.90	2.53
34	off	1.13	3.02	1.19	3.30	1.67	7.49	3.32	2.71	3.50	3.09
z (m)	Foliage	RMSE	R ²	RMSE	R ²	RMSE	R ²	RMSE	R ²	RMSE	R ²
UMBS											
46	on	0.022	0.949	0.020	0.956	0.030	0.897	0.024	0.934	0.025	0.931
46	off	0.019	0.964	0.018	0.968	0.027	0.923	0.021	0.952	0.022	0.948
34	on	0.023	0.952	0.023	0.954	0.033	0.889	0.025	0.935	0.025	0.935
34	off	0.029	0.933	0.029	0.932	0.030	0.913	0.021	0.955	0.022	0.953
MMSF											
46	on	0.027	0.928	0.025	0.939	0.038	0.853	0.029	0.917	0.029	0.916
46	off	0.031	0.909	0.030	0.918	0.031	0.895	0.021	0.950	0.021	0.949
34	on	0.028	0.938	0.027	0.941	0.041	0.864	0.039	0.878	0.039	0.878
34	off	0.028	0.934	0.031	0.923	0.031	0.915	0.028	0.934	0.028	0.934

In practice, the exponent of 2.1 in Equations (21) and (23) has been modified to 2 for an analytical solution to be achieved (Eugster and Senn, 1995; Horst, 1997). Thus, we also used the following equations to fit our data,

$$\frac{n\text{Co}_{uw}(n)}{u'w'} = \frac{\beta_{+5}^{uw}(f/f_0)}{1 + \beta_{+6}^{uw}(f/f_0)^2}, \quad (24)$$

$$\frac{n\text{Co}_{w\theta}(n)}{w'\theta'} = \frac{\beta_{+7}^{w\theta}(f/f_0)}{[1 + \beta_{+8}^{w\theta}(f/f_0)]^2}. \quad (25)$$

where the coefficients β_{+5}^{uw} , β_{+6}^{uw} , $\beta_{+7}^{w\theta}$ and $\beta_{+8}^{w\theta}$ are slightly larger than the corresponding coefficients β_{+1}^{uw} , β_{+2}^{uw} , $\beta_{+3}^{w\theta}$ and $\beta_{+4}^{w\theta}$ in Equations (21) and (23) (Table VI). The only noticeable differences in the normalized cospectra are at the higher frequency end, but the cospectral contributions to the total covariances are generally small in this frequency range (Figure 8).

In both seasons, the coefficients β_{+1}^{uw} and β_{+2}^{uw} at the UMBS site are smaller than those of Kaimal et al. (1972), while the opposite is generally the case at the MMSF site, particularly at the 34-m level. In general, all coefficients are greater at the MMSF site, and so are their variations with height or season (Table VI).

4. Cospectral Corrections of Flux Losses

4.1. DEFINITIONS

The true kinematic vertical eddy-covariance fluxes of a scalar (s) can be expressed as the integral of its true one-sided cospectrum over frequency n ,

$$\overline{w's'} = \int_0^{\infty} \text{Co}_{ws}(n) \, dn, \quad (26)$$

where w' and s' are fluctuations of vertical velocity and scalar concentration, respectively, and the overbar indicates an ensemble average. In practice, the integration is limited by the sampling rate and averaging time.

Similarly, the measured flux and cospectrum, denoted by the superscript m , are:

$$\overline{w's'}^m = \int_0^{\infty} \text{Co}_{ws}^m(n) \, dn = \int_0^{\infty} H_{ws}(n) \text{Co}_{ws}(n) \, dn, \quad (27)$$

where $H_{ws}(n)$ is a net transfer function or the product of a set of transfer functions characteristic of a particular eddy-covariance system and the scalar s (Moore, 1986; Massman, 2000).

A flux attenuation factor (δ_s) can be defined as:

$$\delta_s = \frac{\overline{w's'}^m}{\overline{w's'}} = \int_0^{\infty} H_{ws}(n) \frac{\text{Co}_{ws}(n)}{\overline{w's'}} \, dn \approx \int_0^{\infty} H_{ws}(n) \frac{\text{Co}_{w\theta}(n)}{\overline{w'\theta'}} \, dn, \quad (28)$$

where θ is potential temperature, and it is assumed that the true normalized cospectra of all scalars have the same form and that the cospectra of sensible heat fluxes can usually be measured with adequate accuracy. Thus, knowledge of $H_{ws}(n)$ is needed in addition to the normalized cospectra discussed in the previous section.

4.2. CHARACTERISTICS OF TRANSFER FUNCTIONS

Lenschow and Raupach (1991) and Massman (1991) studied the attenuation of scalar concentrations through tubes as functions of Reynolds number, flow rate, geometry of the tube (inner diameter, length, straight, curved or elbow bend), Schmidt number of the scalar, along with other factors. In practice, such factors, and thus the attenuation, may vary with time. For example, Leuning and Judd

(1996) showed that the attenuation to water vapour by aged and dirty tubes is much greater than that by new and clean tubes.

In this study, we used an empirical approach to evaluate the transfer functions. Using the definitions in Section 4.1, we have,

$$H_{ws}(n) = \delta_s \frac{\left(\frac{CO_{ws}^m(n)}{w's^m}\right)}{\left(\frac{CO_{w\theta}(n)}{w'\theta'}\right)} = \frac{1}{1 + (2\pi\tau_s n)^2}, \quad (29)$$

where the far right-hand side is a form of the transfer function for a first-order sensor, and τ_s is the characteristic time constant of the sensor response (Horst, 1997), which is equivalent to the inductance in an alternating circuit (Eugster and Senn, 1995). We can estimate both δ_s and τ_s through a non-linear fit to Equation (29), using the ratios of measured normalized cospectra of CO₂ or water vapour fluxes to those of sensible heat as a function of frequency n . In practice, this should be done for periods when changes in the transfer function may be assumed to be small. Consequently, the values of δ_s and τ_s represent ensemble averages for each period.

The range of frequency n used for the non-linear fit is determined from ensemble (monthly) averages of measured cospectra of sensible heat, water vapour and CO₂ fluxes (Figure 9, upper panel). Typically, the lower limit is chosen as $n = 0.01$ Hz as the peak frequency is between 0.01 and 0.02, slightly higher (about 0.3) for the nighttime. The higher limit is determined as the ratio of normalized cospectra of water vapour or CO₂ flux to those of sensible heat flux falls below 0.05. The non-linear fit is applied to the ensemble average of these ratios (Figure 9, lower panel); the standard deviations of these ratios change little across the frequency n . This consistency could indicate that the transfer function, and thus τ_s , change little during the period of data shown here. The attenuation is generally greater for water vapour flux than for CO₂ flux (Figure 9, upper panel). This is illustrated also by both lower normalized cospectra at higher frequencies ($n > 0.1$) and the greater cospectral peak (as total covariance is attenuated more).

The characteristic response time (τ_s) for water vapour flux increases each year but not so for the CO₂ flux (Table VII). Note that new tubes were installed at the UMBS site before the growing season in 2001, while the tubes at the MMSF site had not been changed (but were cleaned annually) from 1998 to 2001.

4.3. COSPECTRAL CORRECTION OF CO₂ AND WATER VAPOUR (OR Q_E) FLUXES

Here we use three methods (Horst, 1997) to estimate the flux loss and discuss their relative merits and weaknesses in practice. Methods 1 and 2 estimate the flux attenuation factor δ_s by integrating the product of the derived transfer function and true normalized cospectra so that the true flux can be estimated (Equation (28)).

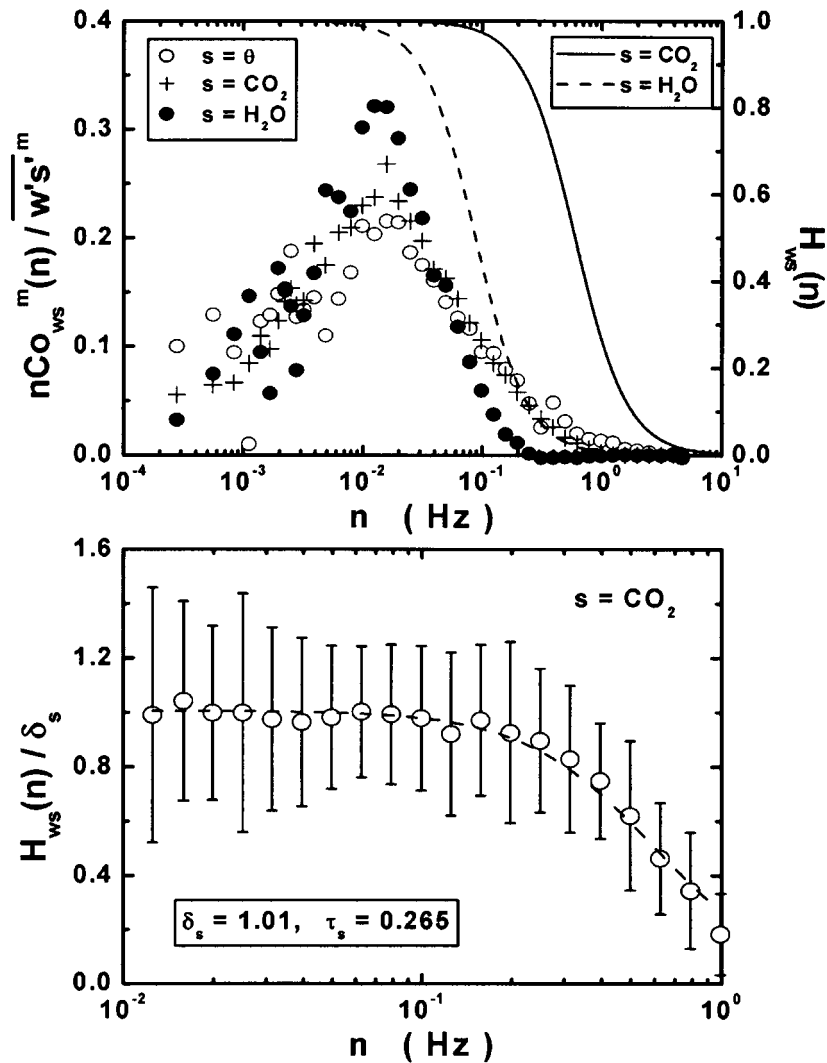


Figure 9. Upper panel: Comparison of normalized cospectra (points) for the vertical water vapour, CO_2 and sensible heat fluxes, and transfer functions (curves) for water vapour and CO_2 fluxes. Lower panel: Non-linear fit to the ensemble average of the ratio between measured normalized cospectra of CO_2 flux and those of sensible heat to the transfer function of a first-order sensor (Equation (29)). Ensemble averaged results for July, 2000 at the 46-m level of the UMBS site during the daytime are shown.

The difference is that Method 1 uses measured normalized cospectra of sensible heat as the true cospectra, while Method 2 takes cospectra models for a particular season at a specific height and site presented in Section 3.3. One weakness of these two methods is that they do not account for any real differences between the model or sensible heat cospectra and water vapour or CO_2 cospectra in the

TABLE VII
Characteristic time constant τ_s (s) (Equation (29)).

Month	UMBS			MMSF			
	1999	2000	2001	1998	1999	2000	2001
CO ₂ flux daytime							
June	0.314	0.256	0.319	0.243	0.325	0.266	0.291
July	0.304	0.265	0.307	0.305	0.299	0.285	0.421
August	0.317	0.278	0.302	0.297	0.284	0.276	0.304
CO ₂ flux nighttime							
June	0.283	0.269	0.306	0.283	0.251	0.214	0.246
July	0.313	0.261	0.305	0.280	0.232	0.299	0.397
August	0.301	0.283	0.286	0.273	N/A	0.284	0.276
Water vapour flux daytime							
June	1.013	1.870	0.532	0.695	2.314	2.658	2.753
July	1.244	1.810	0.673	0.608	2.117	2.536	3.625
August	1.637	2.504	1.024	0.636	1.723	2.668	4.637

lower frequency range, especially for the model cospectra. Such differences in the low frequencies could be relatively large and important at certain conditions (Sakai et al., 2001; Finnigan et al., 2003).

Method 3 simply divides measured cospectra by the transfer function and then integrates them over frequency to obtain the corrected flux (Equations (26) and (27)). An advantage is that this preserves any real variations in the lower frequencies of CO₂ and water vapour cospectra that are essentially not damped, but may be different from the sensible heat flux cospectra or the model cospectra. However, if the cospectra in the highest frequency end are attenuated to the noise level, such noise could be amplified by the transfer function and could introduce an artifact into the flux correction. The same could happen in Method 1, if measurement errors are large in the highest frequencies of the sensible heat flux cospectra. It is much less of a problem in Method 2 when the cospectra model is used.

Thus, for all three methods, we calculated the measured (not corrected) water vapour and CO₂ fluxes as the integration of respective measured cospectra from the lowest frequency to a cut-off frequency at which the normalized cospectra $n\text{Co}_{xy}(n)/\overline{x'y'}$ falls below 0.01 or the transfer function is smaller than 0.1 (Figures 7–9). Hourly data were discarded if the contributions to the total scalar flux above this cut-off frequency estimated using either model cospectra or the measured sensible heat flux cospectra were greater than 50%, as the measured cospectra of water vapour and CO₂ fluxes were considered to be attenuated too much to be deemed reliable for correction in these cases. Then, the normalized cospectra were corrected using the three methods up to this cut-off frequency. The fractional contribution to

the total flux above the cut-off frequency is calculated using the model cospectra in all three methods. For the present study, we used Equation (20) for neutral and unstable conditions to apply Method 2, as it is simpler than Equation (19), and has no discontinuity at $f = 1$. Equation (23) was used for stable conditions. These corrections were applied to measurements from June through August from 1999 to 2001 for the UMBS site, and from 1998 to 2001 for the MMSF site. Transition periods (non-steady state) near sunrise and sunset (small sensible heat flux) are excluded for the correction of CO_2 flux, while only daytime latent heat fluxes were corrected as they are usually very small at night. In the following discussion and related figures, measured CO_2 and latent heat fluxes are denoted by F_{CO_2} and Q_E , respectively, and their corrections by ΔF_{CO_2} and ΔQ_E .

In general, corrections are the largest using Method 3 and the least using Method 1 (Figure 10). The attenuation factor for CO_2 flux δ_{CO_2} changes little from year to year at both sites using the same correction method, except that it is slightly larger (less attenuation) at nighttime in 2000 at the UMBS site. However, the attenuation factor for latent heat flux δ_{Q_E} showed clear year-to-year variations, smallest (greatest attenuation) in 2000 and greatest (least attenuation) in 2001 at the UMBS site (Figure 10a), and continuously decreases from 1998 to 2001 at the MMSF site (Figure 10b). These variations remain the same regardless of the correction method used, and are consistent with the variations in the characteristic time constant for the water vapour flux at the two sites (Table VII). Again, it illustrates that tube attenuation for water vapour fluxes increases greatly with the tubes aging, but not so for CO_2 fluxes.

The attenuations to CO_2 fluxes during the summer period are on average about 3–4% in the day and 6–10% at night (Figure 10). Because the absolute differences during daytime and nighttime have opposite signs (Figure 11), the impact of the cospectral corrections to the cumulative net ecosystem exchange (NEE) during the growing season is reduced due to the partial cancellations. This could also be the case for the gross ecosystem production (GEP) or photosynthetic uptake in the daytime, as it is usually estimated by subtracting ecosystem respiration from NEE, which is measured using the eddy-covariance method. However, such an impact would remain on the ecosystem respiration at nighttime during the growing season, as well as during the dormant season when there is no cancellation. The attenuations to latent heat fluxes are about 20% in 2000, and about 10% in 1999 at the UMBS site (Figure 10a). They were less than 10% in 1998 and over 20% in 2001 at the MMSF site (Figure 10b).

The relatively smaller corrections to CO_2 fluxes generally do not alter their seasonal and annual variability observed before the corrections. For example, daytime CO_2 fluxes during the growing season are the greatest (more negative) in 1999 and least in 2001 at the UMBS site both before and after correction (Figure 11a). This is not the case for latent heat flux. Before correction, Q_E is about 50 W m^{-2} higher in 2001 than in 2000 in midday at the UMBS site, but is about the same for the two years after correction (Figure 11a). For the MMSF site, Q_E is about the same in

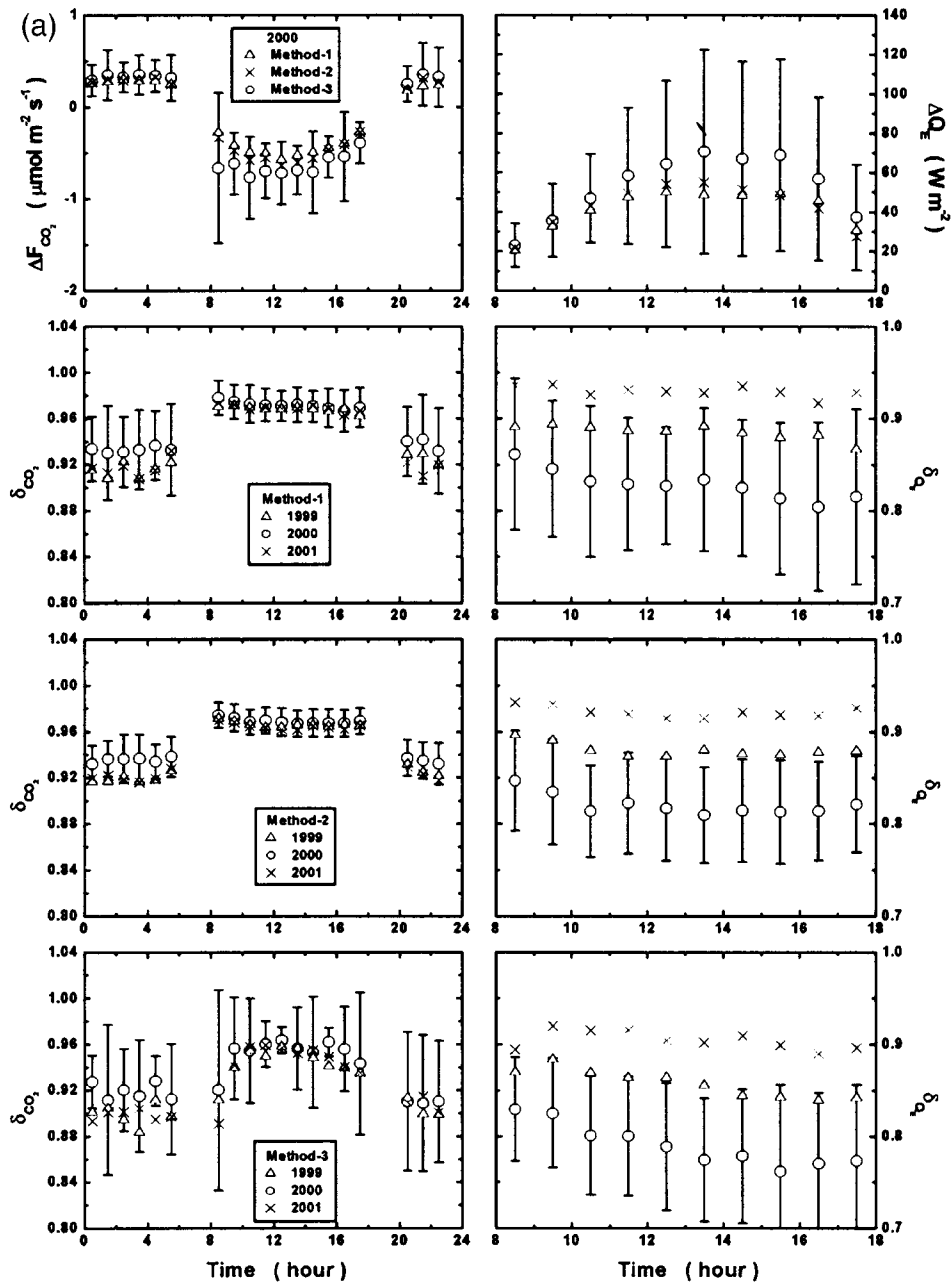


Figure 10. (a) Ensemble average of diurnal courses of CO_2 flux correction ΔF_{CO_2} and latent heat flux correction ΔQ_E , and flux attenuation factors for CO_2 (δ_{CO_2}) and for latent heat flux (δ_{Q_E}). The top panel compares the corrections using the three methods for the same year, whereas the lower three panels illustrate the year-to-year variations for each method. Data shown are for June through August at the 46-m level of the UMBS site. (b) Same as in (a) but for the MMSF site.

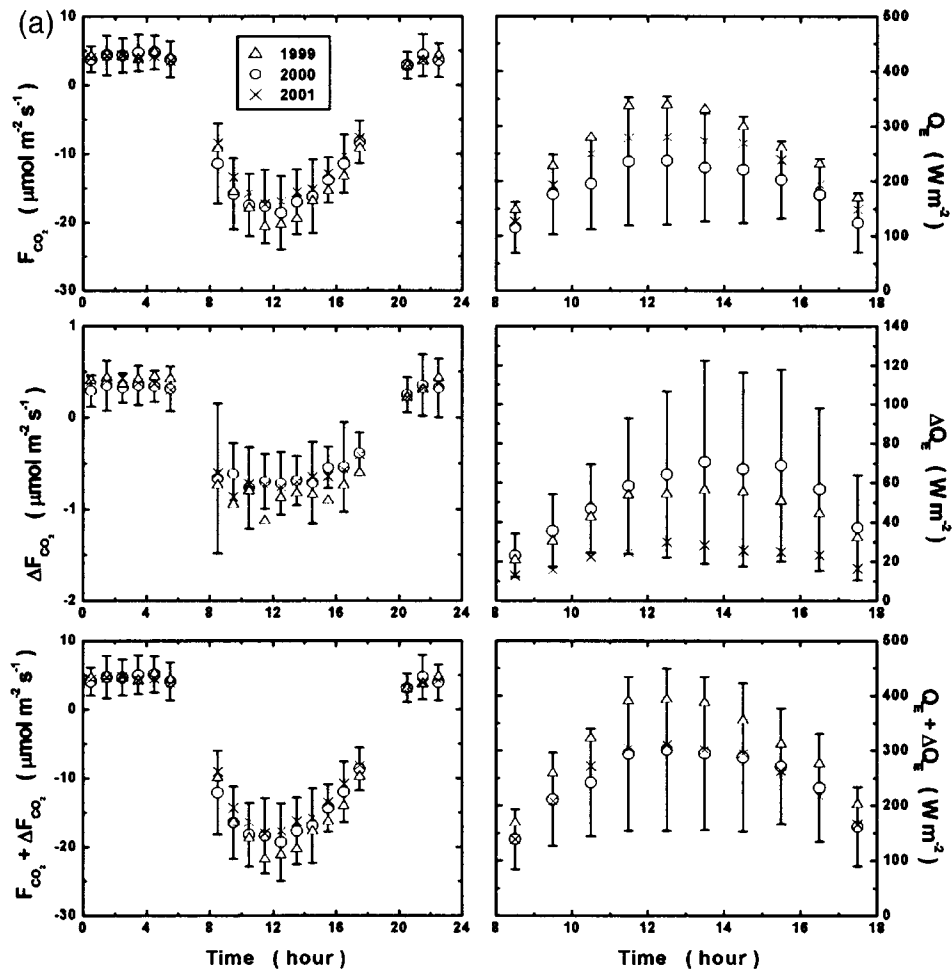


Figure 11. (a) Year-to-year variations in the ensemble-averaged diurnal course of measured CO_2 flux F_{CO_2} and latent heat flux Q_E , their corrections (using Method 3) ΔF_{CO_2} and ΔQ_E , and corrected fluxes. Data shown are for June through August at the 46-m level of the UMBS site. (b) Same as in (a) but for the MMSF site.

all four years (1998–2001) before correction, but exhibits year-to-year variations after correction, least in 1998 and greatest in 2001 (Figure 11b), with a difference of about 100 W m^{-2} at midday.

4.4. EFFECTS ON THE ENERGY BALANCE CLOSURE

The large percentages of correction in latent heat fluxes are expected to have significant impacts on the energy balance. One statistical measure of energy balance closure is the slope of the linear fit (forced through the origin) for $Q_H + Q_E$ versus

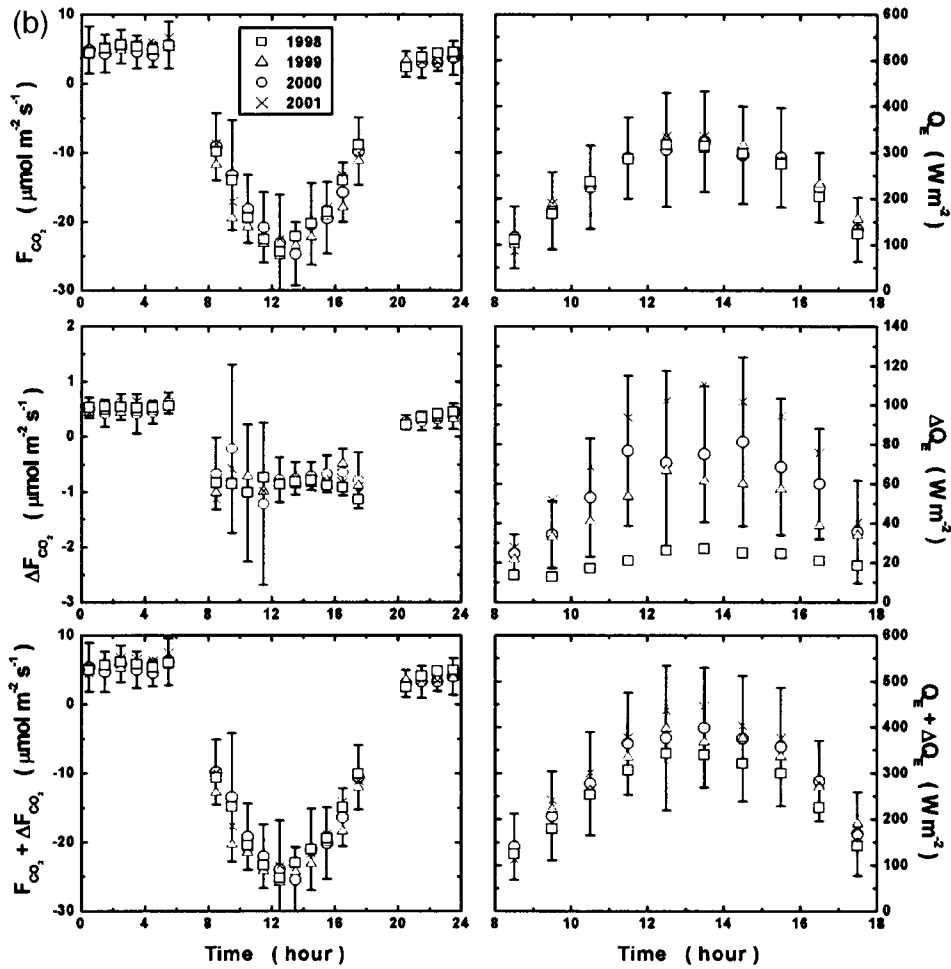


Figure 11. Continued.

$Q^* - Q_G$. Here, we examine the impact of the cospectral corrections in Q_E on this slope as an illustration.

In 2000, before and after correction, this slope was increased from 0.944 to 1.089 at the UMBS site, and from 0.785 to 0.929 at the MMSF site (Figure 12). Such increases vary from year to year and between the two sites (Table VIII), but generally follow the percentage of correction in Q_E (Figure 10). For example, using Method 3 at the UMBS site, the minimum increase is 0.053 in 2001 and maximum is 0.145 in 2000, while at the MMSF site, the minimum increase is 0.046 in 1998 and maximum is 0.187 in 2001. Note that correction Method 3 always yielded the largest increase, and Method 1 the least, for the same period and at the same site.

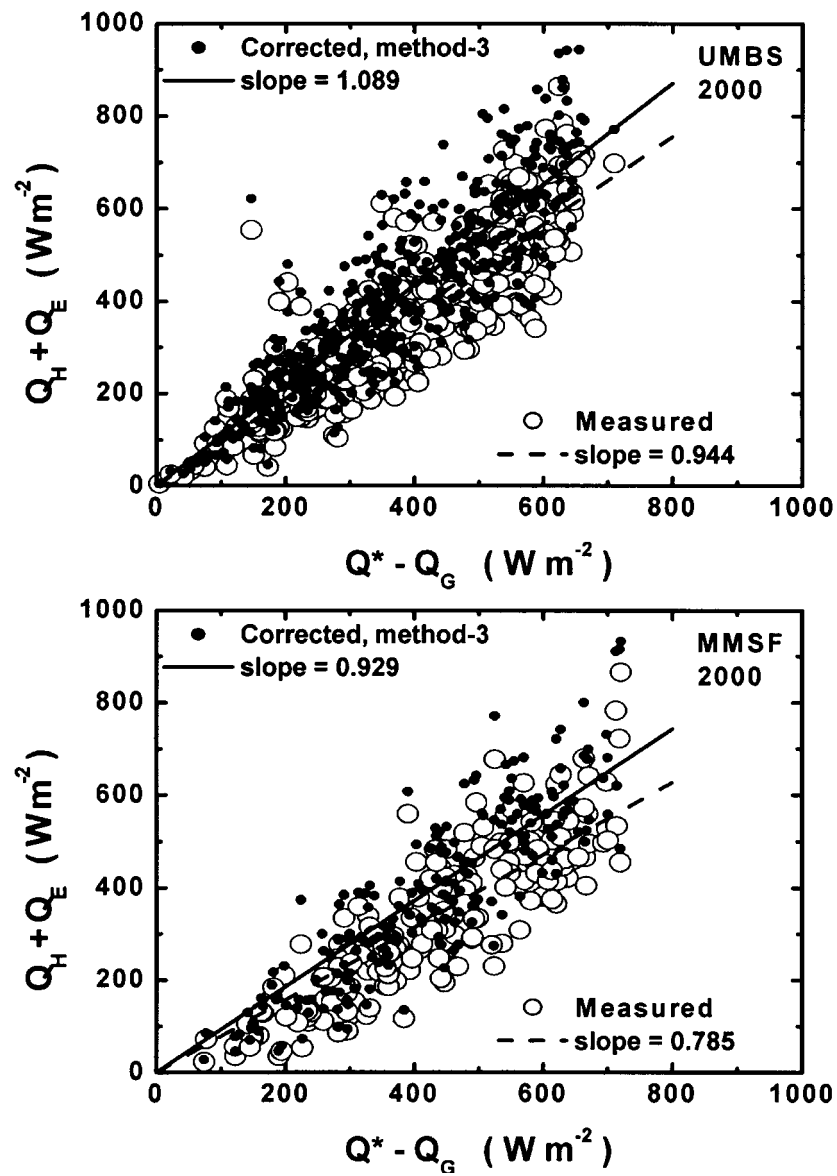


Figure 12. Increases in the slopes of linear fits (forced through the origin) of $Q_H + Q_E$ versus $Q^* - Q_G$ as a result of cospectral correction to Q_E . Data shown are for June through August at the 46-m level in 2000.

TABLE VIII

Impacts of corrections in Q_E on the linear fit (forced through origin) for $Q_H + Q_E$ versus $Q^* - Q_G$ at the 46-m level from June through August at the UMBS and MMSF sites. The coefficient of determination is denoted by R^2 .

Year	1998		1999		2000		2001	
	Slope	R^2	Slope	R^2	Slope	R^2	Slope	R^2
UMBS								
Measured			0.974	0.960	0.944	0.960	0.964	0.956
Method-1			1.059	0.961	1.053	0.960	1.005	0.956
Method-2			1.067	0.960	1.060	0.958	1.012	0.955
Method-3			1.082	0.961	1.089	0.957	1.017	0.956
MMSF								
Measured	0.718	0.949	0.737	0.945	0.785	0.947	0.773	0.941
Method-1	0.753	0.953	0.835	0.951	0.899	0.956	0.919	0.949
Method-2	0.753	0.951	0.836	0.951	0.906	0.952	0.927	0.945
Method-3	0.764	0.953	0.845	0.951	0.929	0.954	0.960	0.943

Even though the cospectral corrections generally increase the slope, and in many cases bring it closer to 1, there are cases where it is still much smaller than 1 or conversely becomes greater than 1. For example, after the correction using Method 3, the slope is only 0.764 in 1998 at the MMSF site, but as large as 1.089 in 2000 at the UMBS site. This indicates that other components of energy budget such as heat storage in the vegetation, measurement errors in Q^* , and corrections to the values of Q_G used here likely have important impacts. These issues are currently under investigation and to be presented elsewhere.

5. Summary and Conclusions

Turbulent spectra and cospectra in the roughness sublayer over two mixed hardwood forests have been analyzed following the approach of Kaimal et al. (1972) for the Kansas experiment. Results presented here are based on nearly 40,000 hours of eddy-covariance measurements at the two long-term AmeriFlux sites at the University of Michigan Biological Station (1999–2001) in northern Lower Michigan and at the Morgan Monroe State Forest (1998–2001) in south-central Indiana.

Although the normalized spectra and cospectra presented here share many similar characteristics to those reported by Kaimal et al. (1972), significant differences were found in both the constants and the stability functions that are needed not only to normalize and to collapse spectra and cospectra in the inertial subrange, but also to derive cospectral model parameters.

Commonalities with the 'classic' spectra and cospectra include the $-2/3$ slope for spectra and $-4/3$ slope for cospectra in the inertial subrange, and the orderly progression towards higher frequency of the spectral and cospectral peak with increasing stability. Similar to Kaimal et al. (1972), we also showed that the cospectra of the vertical sensible heat fluxes differ from those of the vertical momentum fluxes. In the former, the $-4/3$ slope roll-off range starts at a higher normalized frequency f than in the latter. Both cospectra confirmed that larger eddies are relatively more important in transporting momentum than sensible heat, while smaller eddies are relatively more efficient in transporting heat. One difference from Kaimal et al. (1972) is that in the inertial subrange, the ratio of lateral to longitudinal velocity spectra (1.15–1.20) is greater than the ratio of vertical to longitudinal velocity spectra (1.01–1.08), and both are smaller than the $4/3$ value as predicted by isotropy. This result is in agreement with the results previously reported from short-term experiments over forest canopies.

The product of the spectral constant for the longitudinal velocity and the non-dimensional TKE dissipation to the $2/3$ power were calculated from spectral densities in the inertial subrange. The values of this product in neutral conditions, and its change with stability, vary with measurement height and seasonal change in VAI. In unstable conditions, a new form of stability function for the non-dimensional dissipation was derived for flow over forests. Such variations and differences were discussed in terms of the TKE budget in the roughness sublayer over forest canopies. Direct measurements of other budget terms, such as local wind shear production, turbulent transport, and pressure transport are needed to verify the characteristics of the non-dimensional dissipation functions presented in this study.

Cospectral constants for sensible heat and momentum in neutral and unstable conditions presented here are of a similar magnitude to values given in Kaimal et al. (1972) and Wyngaard and Coté (1972), but also showed great variations with measurement height, season and site with different canopy morphology. In stable conditions, a non-linear form of the stability function is proposed to normalize and collapse the cospectra in the inertial subrange. The analysis of Wyngaard and Coté (1972) predicts that these stability functions should be proportional to $\zeta^{4/3}$ in very stable conditions. However, our results showed that such a proportionality varies from $\zeta^{0.49}$ to $\zeta^{0.72}$ for momentum cospectra, and from $\zeta^{0.26}$ to $\zeta^{0.45}$ for sensible heat cospectra. Again, direct measurements of stability functions of non-dimensional shear and temperature gradient in the roughness layer above forest canopies are needed to verify any differences from those used in the analysis of Wyngaard and Coté (1972).

In spite of the differences in spectral and cospectral constants and stability functions, we found that the empirical forms from Kaimal et al. (1972) may be modified to fit the normalized cospectra over forests, providing appropriate cospectral constants and stability functions are used.

The transfer function of a first-order sensor (Eugster and Senn, 1995; Horst, 1997) was fitted to the ratio of cospectra of CO₂ or water vapour fluxes to those of sensible heat to study the characteristics of damping by long tubes. As reported previously by Leuning and Judd (1996), the characteristic time constant for CO₂ cospectra is much smaller than that for water vapour cospectra. The latter also increases greatly with tube aging.

Three methods were compared to estimate the flux attenuation and correction. From June through August, the attenuations of CO₂ fluxes are found to be, on average, about 3–4% during the daytime and 6–10% at night. For latent heat flux during the day, the attenuations range from less than 10% for newer tubes to over 20% for aged tubes.

Corrections to the latent heat flux led to increases in the slope of linear fits (forced through the origin) for $Q_H + Q_E$ versus $Q^* - Q_G$ by up to 0.145 at the UMBS site, and by 0.187 at the MMSF site. For the MMSF site, such increases generally led to a slope closer to, but still less than, 1, and was only improved to 0.764 in 1998. On the other hand, the slope after correction at the UMBS site is up to 1.089 in 2000. Clearly, the cospectral correction for Q_E presented here addresses only one component of the energy balance closure problem, albeit an important one. Corrections of other terms, including the heat storage in biomass, measurement errors in net radiation, and corrections to measured soil heat flux, need to be assessed for a comprehensive treatment of the problem.

Finally, we recognize that effects of longer sampling or averaging periods, detrending or the moving average, cross-talk, line averaging, transducer shadow effects and flow distortions on the spectra and cospectra measured by sonic anemometers are still unresolved issues worthy of further investigation, despite considerable progress since the pioneering days of Kaimal et al. (1972)

Acknowledgements

Funding for this research was provided by the U.S. Department of Energy through its National Institute of Global Environmental Change. We would like to acknowledge the important contributions by Peter Curtis, James Teeri and Brian Bovard in the establishment of the UMBS site, and by Brian Offerle, Ford Cropley and Steve Scott for the MMSF site. Numerous graduate and undergraduate students also contributed to the field and lab research at both sites. A careful review by Dr. Catherine Souch, and comments by two anonymous reviewers, are greatly appreciated.

References

- Amiro, B. D.: 1990, 'Drag Coefficients and Turbulence Spectra within Three Boreal Forest Canopies', *Boundary-Layer Meteorol.* **52**, 227–246.

- Anderson, D. E., Verma, S. B., and Clement, R. J.: 1986, 'Turbulent Spectra of CO₂, Water Vapour, Temperature and Velocity over a Deciduous Forest', *Agric. For. Meteorol.* **38**, 81–99.
- Baldocchi, D. D. and Meyers, T. P.: 1988, 'A Spectral and Lag-Correlation Analysis of Turbulence in a Deciduous Forest Canopy', *Boundary-Layer Meteorol.* **45**, 31–58.
- Baldocchi, D. D., Finnigan, J. J., Wilson, K. B., Paw U, K. T., and Falge, E.: 2000, 'On Measuring Net Ecosystem Carbon Exchange over Tall Vegetation on Complex Terrain', *Boundary-Layer Meteorol.* **96**, 257–291.
- Dwyer, M. J., Patton, E. G., and Shaw, R. H.: 1997, 'Turbulent Kinetic Energy Budgets from a Large-Eddy Simulation of Airflow above and within a Forest Canopy', *Boundary-Layer Meteorol.* **84**, 23–43.
- Eugster, W. and Senn, W.: 1995, 'A Cospectral Correction Model for Measurement of Turbulent NO₂ Flux', *Boundary-Layer Meteorol.* **74**, 321–340.
- Finnigan, J. J., Clements, R., Malhi, Y., Leuning, R., and Cleugh, H. A.: 2003, 'A Re-Evaluation of Long-Term Flux Measurement Techniques Part I: Averaging and Coordinate Rotation', *Boundary-Layer Meteorol.* **107**, 1–48.
- Garratt, J. R.: 1972, 'Studies of Turbulence in the Surface Layer over Water', *Quart. J. Roy. Meteorol. Soc.* **98**, 642–657.
- Garratt, J. R.: 1992, *The Atmospheric Boundary Layer*, Cambridge University Press, Cambridge, U.K., 316 pp.
- Högström, U.: 1990, 'Analysis of Turbulent Structure in the Surface Layer with a Modified Formulation for Near Neutral Conditions', *J. Atmos. Sci.* **47**, 1949–1972.
- Horst, T. W.: 1997, 'A Simple Formula for Attenuation of Eddy Fluxes Measured with First-Order-Response Scalar Sensors', *Boundary-Layer Meteorol.* **82**, 219–233.
- Horst, T. W.: 2000, 'On Frequency Response Corrections for Eddy Covariance Flux Measurements', *Boundary-Layer Meteorol.* **94**, 517–520.
- Kaimal, J. C. and Finnigan, J. J.: 1994, *Atmospheric Boundary Layer Flows: Their Structure and Measurement*, Oxford University Press, Oxford, U.K., 289 pp.
- Kaimal, J. C., Wyngaard, J. C., and Coté, O. R.: 1972, 'Spectral Characteristics of Surface-Layer Turbulence', *Quart. J. Roy. Meteorol. Soc.* **98**, 563–589.
- Lee, X.-H.: 1998, 'On Micrometeorological Observations of Surface-Air Exchange over Tall Vegetation', *Agric. For. Meteorol.* **91**, 39–49.
- Lenschow, D. H. and Raupach, M. R.: 1991, 'The Attenuation of Fluctuations in Scalar Concentrations through Sampling Tubes', *J. Geophys. Res.* **96**(D8), 15259–15268.
- Leuning, R. and Judd, M. J.: 1996, 'The Relative Merits of Open- and Closed-Path Analyzers for Measurement of Eddy Fluxes', *Global Change Biol.* **2**, 241–253.
- Massman, W. J.: 1991, 'The Attenuation of Concentration Fluctuations in Turbulent Flow through a Tube', *J. Geophys. Res.* **96**(D8), 15269–15273.
- Massman, W. J.: 2000, 'A Simple Method for Estimating Frequency Response Corrections for Eddy Covariance Systems', *Agric. For. Meteorol.* **104**, 185–198.
- McMillen, R. T.: 1988, 'An Eddy Correlation Technique with Extended Applicability to Non-Simple Terrain', *Boundary-Layer Meteorol.* **43**, 231–245.
- Moore, C. J.: 1986, 'Frequency Response Corrections for Eddy Correlation Systems', *Boundary-Layer Meteorol.* **37**, 17–35.
- Paw U, K. T., Baldocchi, D. D., Meyers, T. P., and Wilson, K. B.: 2000, 'Correction of Eddy-Covariance Measurements Incorporating Both Advective Effects and Density Fluxes', *Boundary-Layer Meteorol.* **97**, 487–511.
- Raupach, M. R., Coppin, P. A., and Legg, B. J.: 1986, 'Experiments on Scalar Dispersion within a Model Plant Canopy Part I: The Turbulence Structure', *Boundary-Layer Meteorol.* **35**, 21–52.
- Riřmann, J. and Tetzlaff, G.: 1994, 'Application of a Spectral Correction Method for Measurements of Covariances with Fast-Response Sensors in the Atmospheric Boundary Layer up to a Height of 120 m and Testing of the Corrections', *Boundary-Layer Meteorol.* **70**, 293–305.

- Sakai, R. K., Fitzjarrald, D. R., and Moore, K. E.: 2001, 'Importance of Low-Frequency Contributions to Eddy Fluxes Observed over Rough Surfaces', *J. Appl. Meteorol.* **40**, 2178–2192.
- Schmid, H. P., Grimmond, C. S. B., Offerle, B., Cropley, F. D., and Su, H.-B.: 2000, 'Measurements of CO₂ and Energy Fluxes over a Mixed Hardwood Forest in the Midwestern United States', *Agric. For. Meteorol.* **103**, 355–373.
- Schmid, H. P., Su, H.-B., Vogel, C. S., and Curtis, P. S.: 2003, 'Ecosystem-Atmosphere Exchange of Carbon Dioxide over a Mixed Hardwood Forest in Northern Lower Michigan', *J. Geophys. Res.* **108**(D14), 4417, doi:10.1029/2002JD003011.
- Shaw, R. H., Silversides, R. H., and Thurtell, G. W.: 1974, 'Some Observations of Turbulence and Turbulent Transport within and above Plant Canopies', *Boundary-Layer Meteorol.* **5**, 429–449.
- Sorbjan, Z.: 1989, *Structure of the Atmospheric Boundary Layer Meteorology*, Prentice Hall Inc., Englewood Cliffs, NJ, 317 pp.
- Stull, R. B.: 1988, *An Introduction to Boundary Layer Meteorology*, Kluwer Academic Publishers, Dordrecht, 666 pp.
- Su, H.-B., Shaw, R. H., Paw U, K. T., Moeng, C.-H., and Sullivan, P. P.: 1998, 'Turbulent Statistics of Neutrally Stratified Flow within and above a Sparse Forest from Large-Eddy Simulation and Field Observations', *Boundary-Layer Meteorol.* **88**, 363–397.
- Vickers, D. and Mahrt, L.: 1997, 'Quality Control and Flux Sampling Problems for Tower and Aircraft Data', *J. Atmos. Oceanic Tech.* **14**, 512–526.
- Wilczak, J. M., Oncley, S. P., and Stage, S. A.: 2001, 'Sonic Anemometer Tilt Correction Algorithms', *Boundary-Layer Meteorol.* **99**, 127–150.
- Wyngaard, J. C.: 1975, 'Modeling the Planetary Boundary – Extension to the Stable Case', *Boundary-Layer Meteorol.* **9**, 441–460.
- Wyngaard, J. C. and Coté, O. R.: 1971, 'The Budgets of Turbulent Kinetic Energy and Temperature Variance in the Atmospheric Surface Layer', *J. Atmos. Sci.* **28**, 190–201.
- Wyngaard, J. C. and Coté, O. R.: 1972, 'Cospectral Similarity in the Atmospheric Surface Layer', *Quart. J. Roy. Meteorol. Soc.* **98**, 590–603.

Copyright of Boundary-Layer Meteorology is the property of Kluwer Academic Publishing / Academic and its content may not be copied or emailed to multiple sites or posted to a listserv without the copyright holder's express written permission. However, users may print, download, or email articles for individual use.